Geomorphology 463 (2024) 109350

Contents lists available at ScienceDirect

Geomorphology

journal homepage: www.journals.elsevier.com/geomorphology

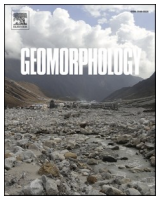

Time-lapse surveys reveal patterns and processes of erosion by exceptionally powerful turbidity currents that flush submarine canyons: A case study of the Congo Canyon

Sean C. Ruffell [a], Peter J. Talling [a,*], Megan L. Baker [a], Ed L. Pope [a], Maarten S. Heijnen [b], Ricardo Silva Jacinto [c], Matthieu J.B. Cartigny [a], Stephen M. Simmons [d], Michael A. Clare [b], Catharina J. Heerema [a,e], Claire McGhee [f], Sophie Hage [c], Martin Hasenhündl [g,h], Dan R. Parsons [i], Shipboard Science Parties on JC187, JC209 research cruises

[a] Departments of Geography and Earth Science, Durham University, Durham DH1 3LE, UK
[b] National Oceanography Centre Southampton, Southampton, Hampshire SO14 3ZH, UK
[c] Marine Geosciences Unit, IFREMER Centre de Brest, Plouzané, France
[d] Energy and Environment Institute, University of Hull, HU6 7RX, UK
[e] Expert Analytics, Møllergata 8, 0179 Oslo, Norway
[f] School of Civil Engineering & Geosciences, Newcastle University, Newcastle upon Tyne NE1 7RU, UK
[g] Institute of Hydraulic Engineering & Water Resources Management, TU Wien, 1040 Vienna, Austria
[h] Institute for Hydraulic Engineering and Hydrometry, Federal Agency for Water Management, 1200 Vienna, Austria
[i] The Loughborough Centre for Sustainable Transitions: Energy, Environment and Resilience, Loughborough University, Leicestershire LE11 3TU, UK

ARTICLE INFO

Keywords:
Submarine canyon
Turbidity current
Erosion
Knickpoint
Mass movement
Geohazard

ABSTRACT

The largest canyons on Earth occur on the seafloor, and seabed sediment flows called turbidity currents play a key role in carving these submarine canyons. However, the processes by which turbidity currents erode submarine canyons are very poorly documented and understood. Here we analyse the first detailed time-lapse bathymetric surveys of a large submarine canyon, and its continuation as a less-deeply incised channel. These are also the most comprehensive time-lapse surveys before and after a major canyon-channel flushing turbidity current. These unique field data come from the Congo Submarine Fan offshore West Africa, where canyon flushing turbidity currents between 2019 and 2020 eroded ~2.65 km^3 of seabed sediment, as they travelled for over 1100 km at speeds of 5–8 m/s. This eroded sediment volume is equivalent to ~19–33 % of global sediment flux from all rivers to the oceans. The time-lapse surveys cover 40 % of the 1100 km long submarine canyon-channel. They show that erosion was predominantly (94 %) along the canyon-channel axis, with only 6 % from failures along canyon or channel flanks. However, erosion along the canyon-channel floor was very patchy; some areas were eroded to depths of 10–20 m, whilst intervening areas showed no significant change. Knickpoints with up-slope migrating headscarps account for 22 % of the total eroded volume. One knickpoint in the deep-sea channel migrated by 21 km in one year, making it the fastest moving submarine knickpoint yet documented. Most (62 %) eroded sediment was in zones extending across the canyon or channel floor, without distinct headscarps as is the case for knickpoints. Erosion restricted to outer bends only comprised 10 % of the total, suggesting processes of erosion differ significantly from meandering rivers in which outer bend erosion is more important. Patchy seabed erosion appears to be mainly due to flow-bed processes (e.g. knickpoints), but spatial variations in seabed sediment properties may also play a role. The irregular seabed erosion occurs despite near-uniform flow speeds observed between moorings and submarine cable breaks with spacing of tens to hundreds of kilometers. Patchy and localised erosion has important implications for assessing hazards to seabed telecommunication cables, which are more likely to break in areas of deep erosion, and for creating appropriate numerical models of seabed erosion and turbidity current behaviour, or how to interpretate ancient submarine canyons and channels in rock outcrops.

* Corresponding author.
E-mail address: Peter.J.Talling@durham.ac.uk (P.J. Talling).

https://doi.org/10.1016/j.geomorph.2024.109350
Received 22 March 2024; Received in revised form 16 July 2024; Accepted 17 July 2024
Available online 26 July 2024

1. Introduction

The deepest canyons on Earth occur on the seafloor (Normark and Carlson, 2003), and these submarine canyons can lead to submarine channels whose dimensions can rival or exceed those of largest terrestrial river systems (Peakall and Sumner, 2015). Sediment that is flushed through these submarine canyon-channels forms the largest sediment accumulations on Earth, called submarine fans, which also produce unusually thick sedimentary sequences within the ancient rock record (e.g. Normark et al., 1993; Hodgson et al., 2011; Hubbard et al., 2020).

Powerful seafloor flows of sediment (turbidity currents) play a critical role in forming and maintaining both submarine canyons (Paull et al., 2018), and less-deeply incised submarine channels (Peakall and Sumner, 2015). These turbidity currents can be generated by disintegration of seafloor landslides, which may themselves excavate canyon walls, as well as by sediment plumes from river mouths and other processes (Talling et al., 2023). Turbidity currents include the longest sediment flows on Earth, sometimes travelling for hundreds or even thousands of kilometers and reaching speeds of 5–19 m/s (Piper et al., 1999; Talling et al., 2022, 2023). These flows can be subdivided into two types (Parker, 1982; Piper and Savoye, 1993; Canals et al., 2006; Talling et al., 2012; Allin et al., 2016). 'Canyon-filling' turbidity currents terminate within canyons, and although they can locally erode sediment, they deposit all of their sediment within the canyon. It is much more powerful and infrequent 'canyon-flushing' turbidity currents that primarily erode and carve submarine canyons, and transfer sediment beyond the end of submarine channels (Normark and Piper, 1991; Allin et al., 2016; Heijnen et al., 2020, 2022; Talling et al., 2022). The volume of sediment carried in canyon-flushing events may be orders of magnitude larger than canyon-filling events (Allin et al., 2016; Mountjoy et al., 2018; Talling et al., 2022).

Although it is known there is a general link between turbidity currents and submarine canyon-channel formation, the detailed processes by which seafloor erosion actually occurs are very poorly documented and thus understood. This knowledge gap reflects a lack of detailed information on patterns and processes of seabed erosion by turbidity currents, especially the most powerful and important canyon-flushing events. The study presented here is important because it provide a detailed analysis of the first bathymetric surveys before and after major canyon-flushing turbidity currents, which were collected in the Congo Submarine Canyon and Channel in 2019 and 2020 (Talling et al., 2022). A small number of previous studies have directly recorded how smaller canyon-filling turbidity currents remould the seabed, such as in Monterey Canyon in California (Paull et al., 2018; Wang et al., 2020; Wolfson-Schwehr et al., 2023) or Canadian fjords (Clare et al., 2016; Hughes Clarke, 2016; Hage et al., 2018). However, the only previous time-lapse surveys available for major canyon flushing turbidity currents were restricted to the uppermost part of Kaikōura Canyon offshore New Zealand (Mountjoy et al., 2018), and this study lacked direct measurements of associated flows. Here we analyse bathymetric surveys along the length of the Congo Submarine Canyon and Channel system offshore West Africa, collected before and after major canyon flushing turbidity currents in 2019 and 2020. A detailed array of moored sensors along this canyon-channel system also directly monitored these canyon-flushing flows, showing they travelled for >1100 km with frontal speeds of 5–8 m/s (Fig. 2; Talling et al., 2022). This unique combination of time-lapse bathymetric surveys and direct monitoring of canyon-flushing flows is used to understand patterns and processes of erosion.

It is important to understand how turbidity currents erode the seabed for a series of reasons. The exchange of sediment between a turbidity current and the seabed (i.e. erosion and deposition) is fundamental to understanding how turbidity currents behave and evolve. This is because erosion effects the density of a turbidity current, which is the driving force behind the flow. For example, if a turbidity current erodes more sediment, it can become denser and thus faster, which may then lead to further erosion and acceleration. This positive feedback has been termed ignition (Parker, 1982). Conversely, if sediment is deposited from a turbidity current it may become less dense, such that it decelerates and dissipates. It has also been proposed that turbidity currents can exist in a third state termed autosuspension, with no net exchange of sediment from the turbidity current to the seabed, such that the flow's density and speed remain nearly constant (Parker et al., 1986; Stevenson et al., 2015; Heerema et al., 2020). These processes of sediment exchange with the bed can therefore dominate overall turbidity current evolution, and they are arguably the most significant uncertainty for numerical modelling of turbidity currents (see Traer et al., 2012).

Understanding how turbidity currents erode the seabed is also important for assessing and mitigating hazards to networks of seabed cables (Carter et al., 2009; Sequeiros et al., 2019), which now carry over 95 % of intercontinental data traffic (Carter et al., 2009). A better understanding of hazards faced by submarine cables is essential due to their increasing economic, societal, and strategic importance (Carter et al., 2009, 2014). Unlike cable breaks due to ship anchors, a single turbidity current can damage multiple seabed cables spread over very large areas. This makes it harder to repair cable faults due to turbidity currents, as repair ships have to repair multiple cables. For example, it took 20–25 days to repair cable breaks offshore West Africa due to turbidity currents that travelled down the Congo Canyon-channel in January and March 2020 (Talling et al., 2021). To assess and mitigate hazards to cables from turbidity currents, it is essential to understand the patterns of erosion and deposition in submarine canyons. This will allow cable companies to lay their cables in lower risk zones, potentially prolonging the lifespan of the cable.

Time-lapse surveys that document patterns and processes of erosion and deposition in modern submarine canyon and channel systems also help to understand and interpret ancient deposits within the rock record. For example, these time-lapse surveys can show how deposits are built up and eroded, and thus stratigraphic completeness, at least over short (near-annual) time scales (e.g. Vendettuoli et al., 2019). Studies such as the one presented here also help to understand the significance and distribution of erosion surfaces within ancient rock sequences, including their role in bypassing extremely large sediment volumes to down-slope areas (e.g. Stevenson et al., 2015).

1.1. Aims

The overarching aim is to understand processes of erosion and sediment exchange between turbidity currents and the seabed, using the Congo Canyon – Channel system as a case study. The first objective is to document the pattern of erosion caused by canyon-flushing turbidity currents, and thus identify different erosional processes. Erosional processes are found to include knickpoint migration, outer-bend erosion, general erosion across the canyon or channel floor ('general thalweg erosion'), and sidewall collapse. The second objective is to determine the volume of erosion resulting from each erosional process, and thus their relative importance. The third aim is to understand what controls the distribution of erosional processes, and the likelihood they occur at a given location. The final objective is to understand wider implications of this study for assessing and mitigating hazards to seabed cables, interpreting ancient canyon and channel deposits in the rock record, and for numerical modelling of turbidity currents.

2. Background to the Congo Submarine Canyon and Channel

The Congo Canyon and Channel extends for >1000 km from the mouth of the Congo River offshore West Africa (Fig. 1). The term 'canyon' denotes areas of especially deep erosion that may contain terraces, whilst 'channel' indicates a less deeply eroded feature, whose external levees are raised above the surrounding seabed (e.g. Babonneau et al., 2002, 2010; and see Fig. 1a for where the terms are used herein). The transition from a canyon to channel is often gradational.

The head of the Congo Canyon lies within the estuary of the Congo

River (Fig. 1), which has the second largest water discharge and fifth largest particulate organic carbon export of any river globally (Coynel et al., 2005). The Congo Canyon is one of the few modern-day submarine canyons that is directly connected to a river, although such direct connections would have been much more common during previous low-stands in sea-level (Covault and Graham, 2010). The Congo River supplies ~29–43 Mt/yr of fine grained sediment that forms a surface plume in the estuary, with early work suggesting it may also carry up to 130 Mt/yr of additional sandy bedload to the canyon head (Peters, 1978), although these estimated sediment fluxes have high uncertainty.

The Congo Canyon is deeply incised into the continental shelf from the mouth of the Congo River, and it transitions into the less incised Congo Channel (Fig. 1; Babonneau et al., 2002, 2010). The Congo Channel terminates at ~4800 m water depth, beyond which there is an area of deposition termed a lobe (Dennielou et al., 2017). The location of the active channel has changed due to repeated avulsions (Picot et al., 2016, 2019). These submarine channel systems and their associated lobes, together with the Congo Canyon, form the well-studied Congo Submarine Fan (e.g. Babonneau et al., 2002, 2010; Anka and Séranne, 2004; Ferry et al., 2004; Savoye et al., 2009; Vangriesheim et al., 2009; Rabouille et al., 2017; Dennielou et al., 2017).

2.1. Direct monitoring of turbidity currents

This study is based on detailed swath multibeam bathymetry surveys collected in September 2019 and September–October 2020, which cover ~40 % of the Congo Canyon-channel (Fig. 1). The 2019 and 2020 cruises surveyed the same reaches of the upper canyon (Fig. 1b) and distal submarine channel (Fig. 1c), allowing time-lapse analysis of seabed change. The 2019 and 2020 cruises also deployed and recovered a variety of turbidity current monitoring equipment, which are important for this study because they document the nature of flows that caused seabed change between the 2019 and 2020 bathymetric surveys (Fig. 2). This included Acoustic Doppler Current Profilers (ADCPs) located on moorings in the thalweg of the canyon and channel (Talling et al., 2021, 2022).

These ADCPs and cable breaks were previously used to document the frontal (transit) speeds, runout distances and number of turbidity currents that occurred between the 2019 and 2020 bathymetric survey (Fig. 2b; Talling et al., 2022). Between October 10th 2019 and 14th January 2020, 12 relatively short runout flows occurred in the proximal part of the Congo Canyon, some 100–200 km from the mouth of the Congo River (Fig. 2a). As these flows terminated within the upper canyon and failed to reach the lobe, they are interpreted as smaller 'canyon filling' events. Three of the ADCP-moorings were broken by these canyon filling flows (Fig. 2a).

The 14th–16th January flow was the first 'canyon flushing' turbidity current in the study period, and it had a runout distance of >1100 km (Fig. 2; Talling et al., 2022). This powerful event caused the remaining eight moorings to surface sequentially, and broke the WACS and SAT-3 telecommunication cables (Figs. 1 and 2a; Talling et al., 2022).OBS and cable breaks recorded a second 'canyon flushing' turbidity current on

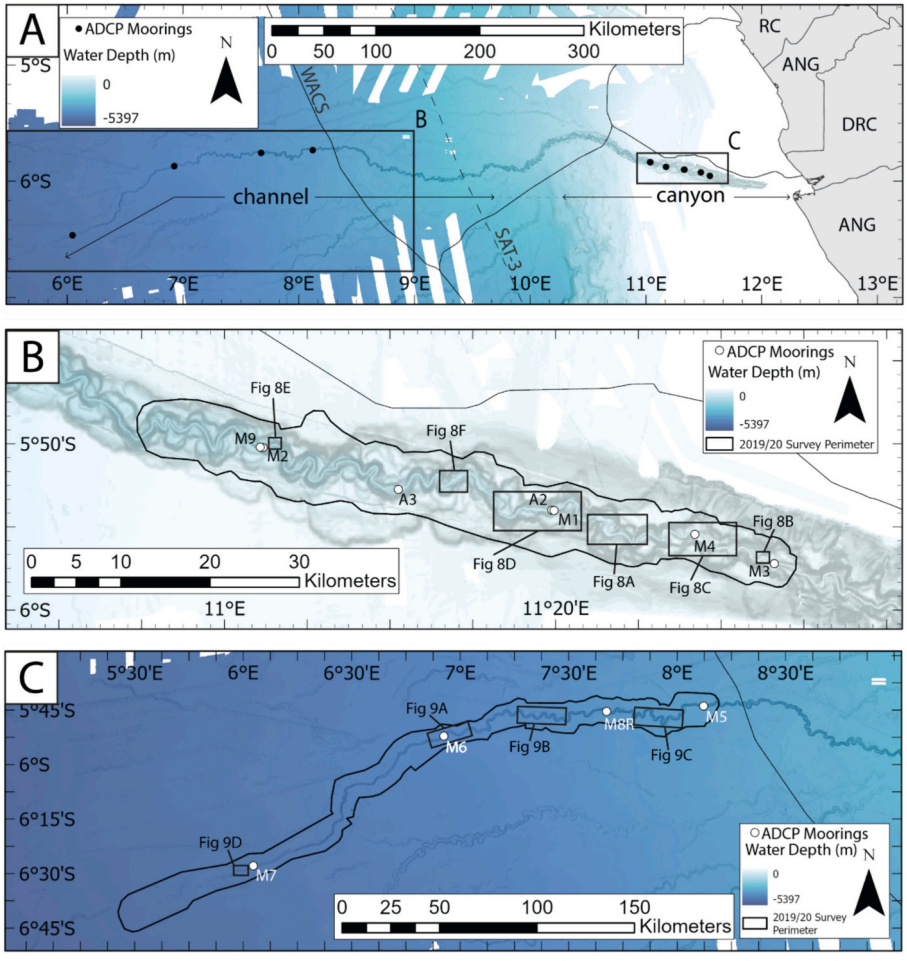

Fig. 1. (A) Overview of the Congo Submarine Canyon and Channel, with Acoustic Doppler Current Profiler (ADCP) mooring locations and WACS and SAT-3 cable routes. Full survey and seabed gradients from the ZaïAngo Project (Savoye et al., 2000). RC is the Republic of the Congo, ANG is Angola, and DRC is the Democratic Republic of the Congo. B) Detailed map of the Congo Submarine Channel. Black outline denotes the 2019 and 2020 survey extent. C) Detailed map of the Congo Submarine Canyon. Black outline denotes the extent of 2019 and 2020 surveys.

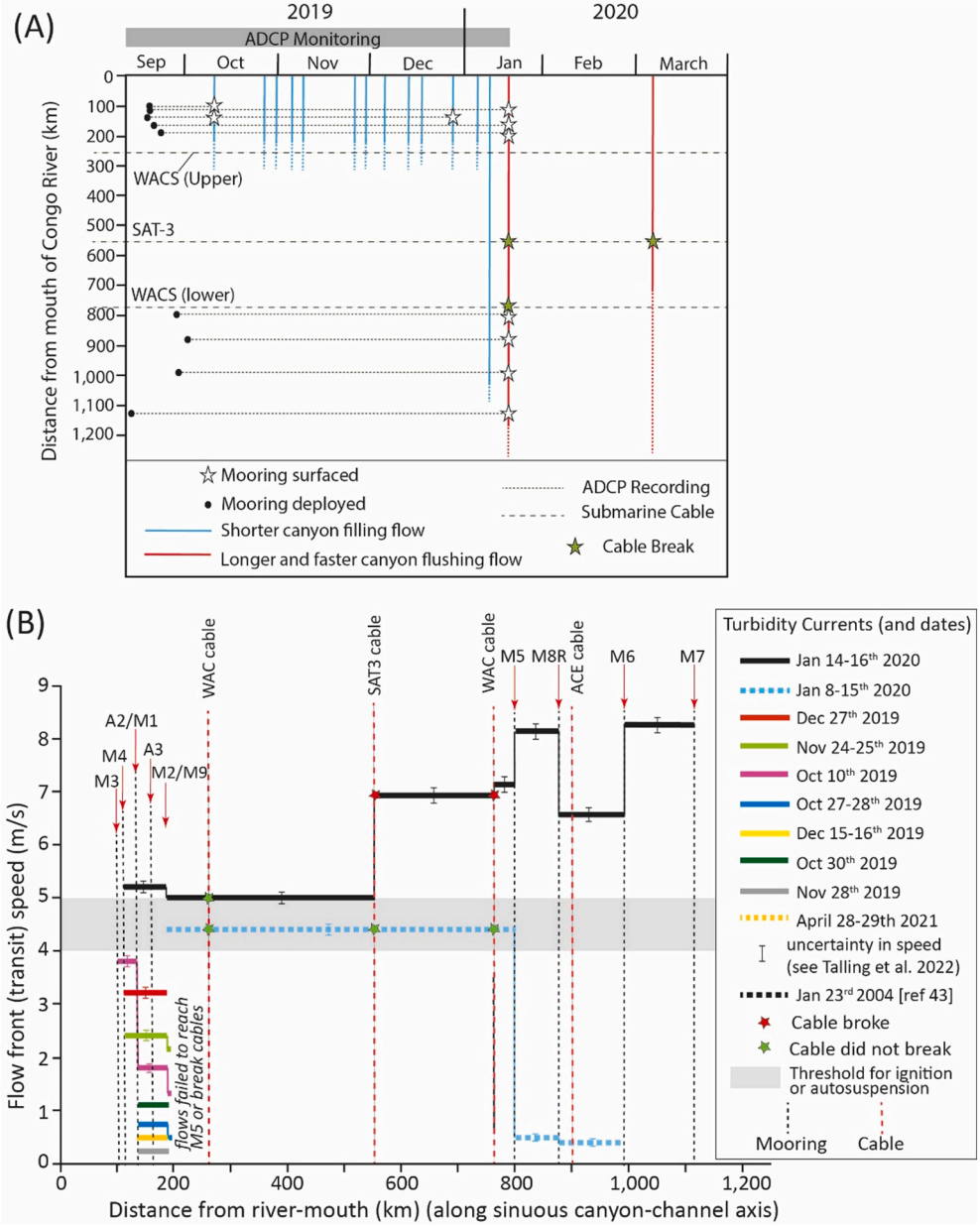

Fig. 2. Turbidity currents monitored between September 2019 and March 2020. (a) Plot shows the date and runout distance (in kilometers from coast) of canyon filling flows (blue lines) and large canyon flushing flows that occurred on January 14-16th and March 9th 2020 (red lines). Data gathered from ADCP moorings and cable breaks. Figure adapted from Talling et al. (2022). (b) Plot shows changes in flow front speed with distance for turbidity currents in the Congo Canyon-channel that occurred from September 2019 to January 2020. Flow front speeds derived from arrival times at moorings and cable breaks. Plot adapted from Talling et al. (2022).

March 8th 2020, which also broke the SAT-3 cable (Talling et al., 2021, 2022). Overall, this has resulted in the Congo Canyon and Channel having both the most detailed time lapse seabed surveys and flow monitoring data for any deep-sea canyon-channel system.

2.2. Total volumes of sediment and organic carbon eroded in 2019–2020

Talling et al. (2022) previously showed that the monitored flows in 2019–2020 eroded a sediment volume of ~2.65 km^3, equivalent to 19–35 % of the global sediment flux from all rivers to the ocean (Syvitski et al., 2022). Presumably, most of this erosion occurred in the two powerful canyon-flushing flows on January 14-16th 2019 and March 8th 2020 (Fig. 2). In this contribution we seek to understand how such a globally significant amount of sediment was eroded.

Ten sediment cores were also collected in 2019, and they provide insights into the types of deposit that were eroded at these core sites between 2019 and 2020. The cores from the canyon were previously used by Baker et al. (2024) to estimate that the eroded material contained 43 ± 15 Mt. of terrestrial organic carbon from the whole canyon-channel system, equivalent to 22 % of the annual global particulate organic carbon export from rivers to oceans, and 54–108 % of the predicted annual terrestrial organic carbon burial in the global oceans. This study also helps to understand how that globally significant amount of organic carbon was re-excavated.

3. Material and methods

3.1.1. Bathymetry surveys in 2019 and 2020

Bathymetric survey data were collected using the Kongsberg EM122 deep water swath multibeam echosounder located on the hull of the vessel. The highest resolution results were obtained by setting the swath to the narrowest setting with a beam angle of 45° from the nadir, with a minimum possible beam angle of 5°, and a survey speed of 6 knots. These surveys covered the floor of the upper canyon within Angolan waters, and the distal submarine channel (Fig. 1). Surveys in September–October 2019 and October 2020 covered the same sections of the canyon-channel system.

These bathymetric data were processed using CARIS Hips and Sips onboard the RRS James Cook, during the surveys. They were corrected for tides, waves, ship motion, and differences in sound velocity of the water. Data for this calibration were obtained from Sound Velocity Profiler dips carried out during the surveys. Bathymetric data in the upper Congo Canyon were gridded at 5 m resolution (Fig. 1c), whilst the deep-water Congo Channel was gridded at 15 m (Fig. 1b).

3.1.2. Changes in seabed elevation (difference maps) from 2019 to 2020

Patterns of seafloor change between the 2019 and 2020 survey data were calculated in ArcGIS PRO. This was done by subtracting the 2020 survey elevations from the 2019 survey elevations, for each grid cell, to create a difference map showing seabed change (Fig. 3). A false colour is applied so that areas in red show erosion, and areas in blue show deposition (Fig. 3C). To determine seafloor erosion for certain features, polygons were drawn manually around erosional or depositional features and assigned a category (Flank Collapse, General Thalweg, Outer Bend, Knickpoint; see Section 4.3 for description of categories). When drawing the polygons, an area of zero elevation change between the outer perimeter of erosion/deposition and the boundaries of the polygon was included (Fig. 3D). This provides a 'no change' buffer around the erosional or depositional features where possible. This was done to ensure there is as little human-induced error as possible when defining the boundaries between erosional and depositional features. In some cases, features came into contact with one another, such as a flank collapse that overlaps the channel floor. In this case, a qualitative boundary between the two must be drawn manually to categorise types of erosion or deposition.

3.1.3. Volumes of seabed change and their uncertainties

Thicknesses of seabed erosion or deposition were multiplied by grid cell areas to quantify volumes of seabed change. The methods of Mountjoy et al. (2018) were chosen for reporting volumes of seabed change, whilst considering recommendations from Schimel et al. (2015). Changes in volume are reported as X [>Y], where X is the most likely value, based on changes in seabed elevation measured at grid cells, whilst Y is a minimum estimate for the eroded volume. The most likely value (X) assumes errors are close to being symmetrically distributed around zero, and thus tend to cancel each other out. Fig. 4 provide an analysis of changes in seabed elevation in areas where no change is expected, such as in overbank areas or terraces away from recent flows (also see Talling et al., 2022). This analysis found measurement uncertainties are symmetrically distributed broadly around a near-zero value (Fig. 4; and see Talling et al., 2022 and Supplementary Figs. 1 and 2).

We also report a minimum estimate for volume of seabed change (Y), which is calculated using a spatially variable limit of detection (also see supplementary material in Talling et al., 2022). If seabed change in a grid cell does not exceed this limit of detection, then the grid cell is not used to calculate the total volume of seabed change. This method is based on spatially variable uncertainties, which vary for each grid cell and are calculated using the CUBE algorithm (Combined Uncertainty and Bathymetric Estimator). The benefits of using CUBE are that this method accounts for a wide array of variables, including: the survey

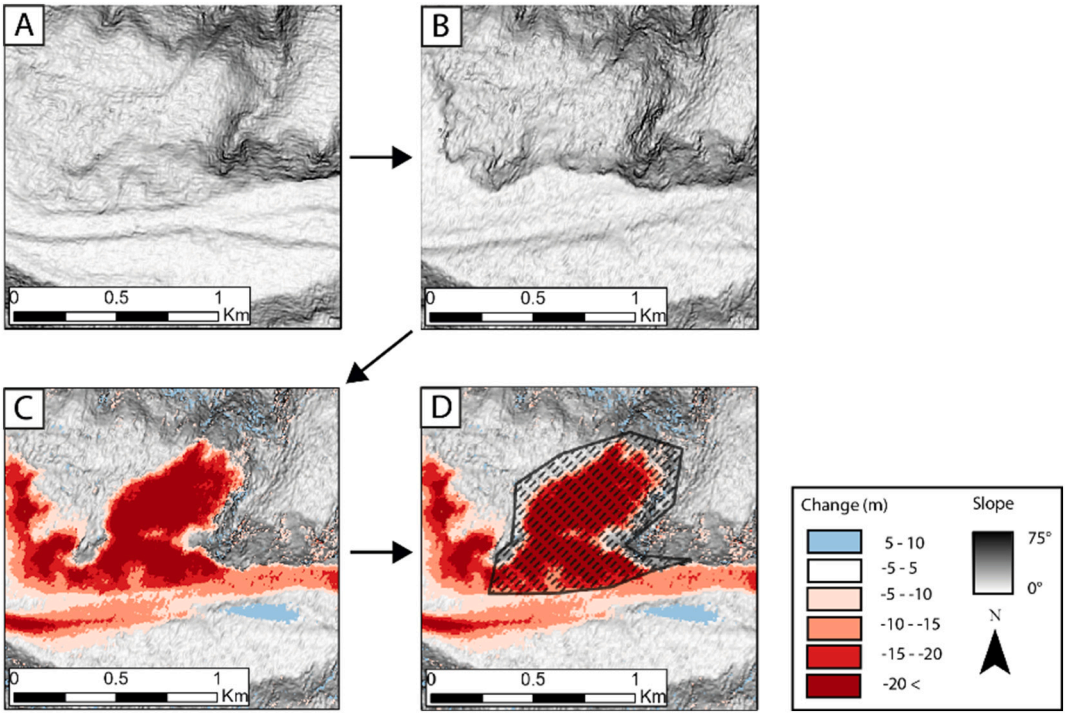

Fig. 3. Workflow of erosion categorisation and volume calculations. A``) Map of seabed gradient for an area of the Congo Canyon in 2019. B) Map of seabed gradient for the same area shown in A, but in 2020. C) Difference map created by subtracting the seabed elevation surveyed in 2019, from seabed elevation surveyed in 2020. Resulting areas of erosion are highlighted in shades of red, and areas of deposition highlighted in shades of blue, with this example showing both flank collapse and channel erosion. D) A polygon is then manually drawn around an individual area of change assigned to a particular category, in this case a flank collapse. This polygon then forms the limits of individual volume calculations for each particular category of erosion.

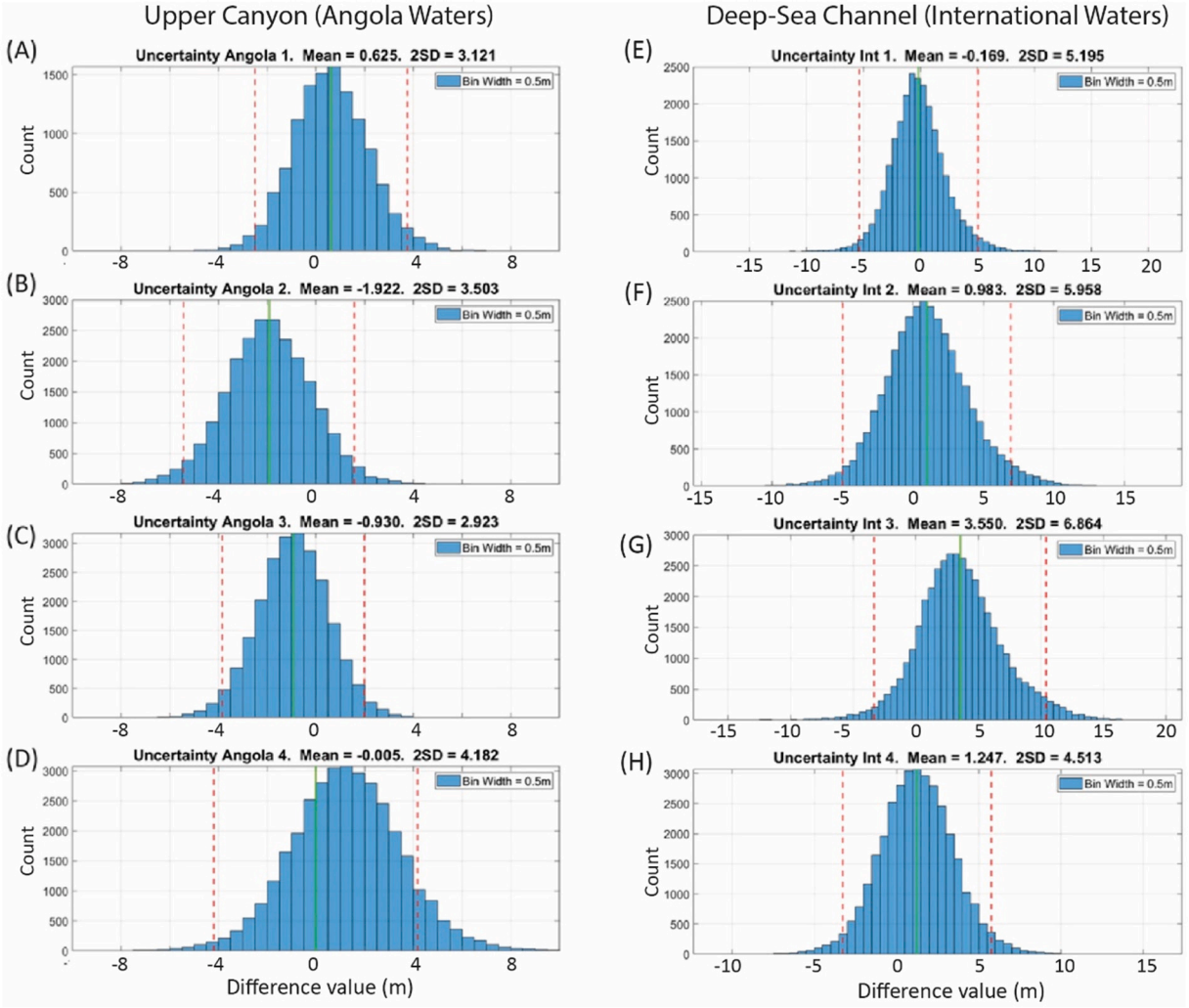

Fig. 4. Measured differences in seabed elevation for areas where no significant (<0.5 m) seabed change was expected, which thus provide an estimate of uncertainties in bathymetric survey data. (a-d) Change in seabed elevation for areas outside the axis of the upper canyon from 2019 to 20. (e-h) Change in seabed elevation for areas outside the deep-sea channel from 2019 to 20. See Supplementary Figs. 1 and 2 for locations of these areas, and Talling et al. (2022) for more details of analyses.

system used, its auxiliary sensors, configuration and conditions of operation, sounding depth, sound velocity, bottom detection algorithm, seabed slope, sounding density and sounding distance from the DEM grid nodes (Calder and Mayer, 2003; Schimel et al., 2015). The spatially variable uncertainty of the difference map is calculated as the propagation in quadrature of the uncertainty of each DEM (to ensure all values are positive), with each cell having a unique uncertainty value assigned (Schimel et al., 2015). CUBE derived uncertainty values are typically <5 m in the shallower-water area in the Congo Canyon, or 10–15 m in the deep-water Congo Channel. The upper limits of these values are broadly comparable to uncertainty values obtained in supplementary Figs. 1 and 2 (and see discussion in Talling et al., 2022).

Each CUBE-derived uncertainty value is then multiplied by a constant 'k', which is the confidence level. A conservative value of $k = 1.96$ was used by Mountjoy et al. (2018) to define their limit of confidence (two standard deviations or 95 % confidence limits). For the purpose of this study a value of $k = 1$ is chosen, which results in the raw uncertainties values calculated by CUBE being used as the final limit of detection, as this more closely reflects uncertainty values calculated with other methods highlighted in Talling et al. (2022). Higher values of k result in a higher threshold that seabed change is real; however, they also result in more grid cells being discarded. A sufficiently high value of k will result in 100 % confidence that at least zero seabed change has occurred, which, whilst correct, is not a useful conclusion (Schimel et al., 2015). We consider the CUBE method with $k = 1$ to be robust approach to calculate the volume of seabed change. However, caution should be taken when interpreting flank collapse eroded volume results. This is because on these steep canyon-flank areas, a small change in seabed elevation (including due to positioning error for the vessel) can produce large errors in seabed elevation and hence estimated eroded volumes. For this reason, flank collapses have only been included in the analysis if they make geological sense (i.e. their outline shape resembles a landslide). Any side wall erosion features that do not look realistic, or look like error in data collection, are discarded from the calculation. This is not the case with the various types of channel floor erosion, as we are more confident that data from the channel floor is representative of true seafloor change. Therefore, other than flank collapses, all other volume calculations have been selected quantitatively to ensure repeatability within this dataset, and for comparison with other datasets.

To enact this CUBE based method for minimum eroded volumes, polygons are run through a model in ArcGIS Pro that (i) creates a mask of the underlying difference map and the combined CUBE uncertainty map for each polygon, and (ii) exports each difference map and combined CUBE uncertainty map as a .txt file. This creates a spatially variable uncertainty map. This map can be used to create a spatially variable

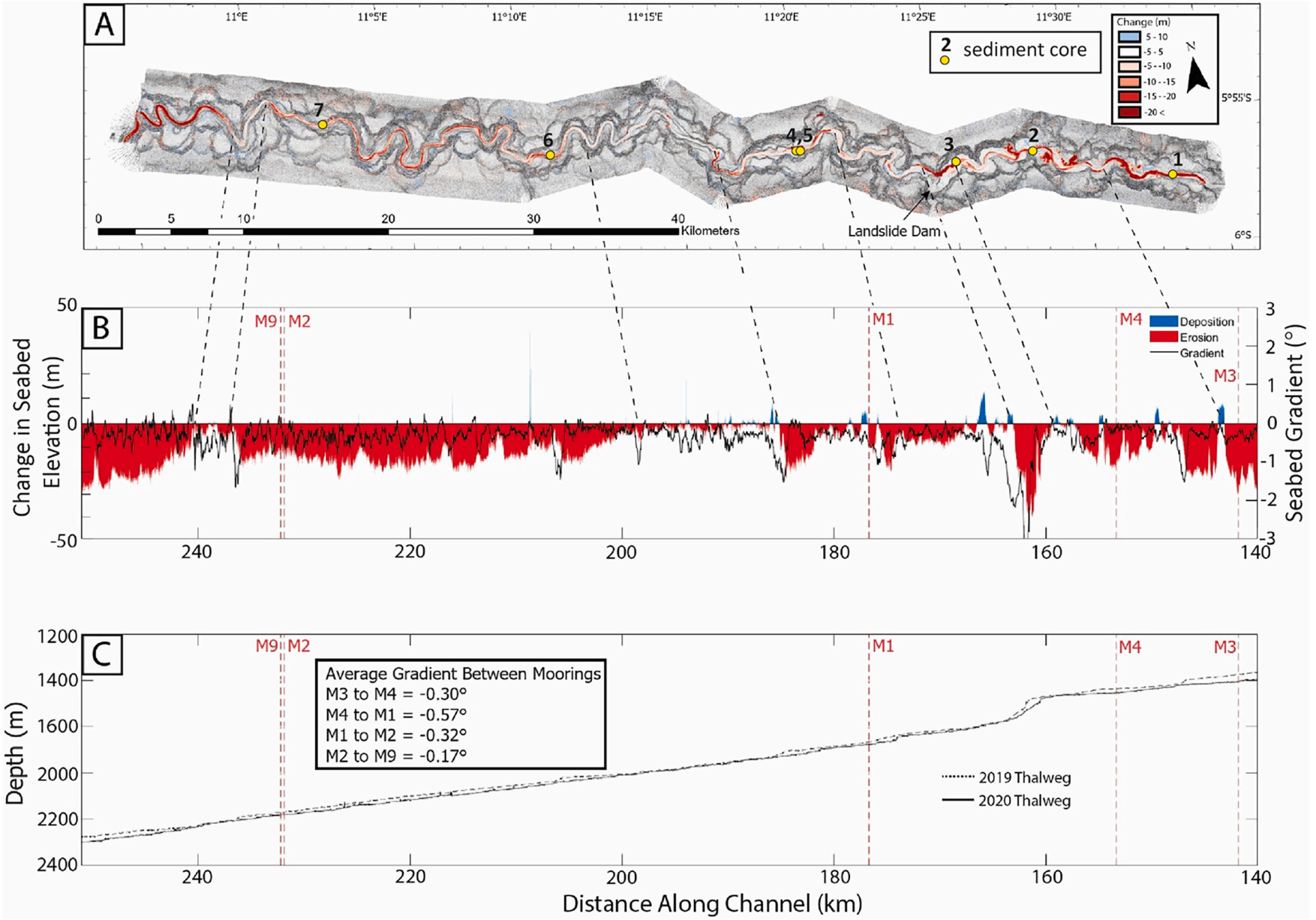

Fig. 5. (below). A) Difference map showing seabed changes within the surveyed area (Fig. 1) of the Congo Canyon. Note the increase in erosion above the annotated landslide dam described in Pope et al. (2022b). Sediment cores sites in 2019 (Figs. 9 and 10) are shown by yellow circles. B) Vertical change in seabed elevation along the thalweg of the canyon between September 2019 and September 2020, plotted with the 2019 thalweg seabed gradient. C) Long profile of the canyon thalweg in 2019 and 2020. Mooring locations used to monitor turbidity currents are indicated with vertical red dashed lines.

limit of detection, so that we can discard volumes of change that are below a grid cell's individual uncertainty. The difference map and combined CUBE uncertainty map .txt files are then imported into MatLab, where they are concatenated into a single table, with each grid cell having its own row showing vertical elevation change in metres and combined uncertainty threshold in metres. If the change exceeds the combined uncertainty, then the change value is kept. If the grid cell change is less than the combined uncertainty, the grid cell is discarded.

To obtain volumes, the remaining difference values are then multiplied by the grid cell resolution. For example, if there is a 5 m horizontal resolution for bathymetry grid cells, then the vertical change is multiplied by 25 m (5 × 5 m), which provides the volume change for each cell in m^3.

3.2. Conversion of sediment volume to sediment mass

Volumes of eroded sediment (km^3) along the Congo Canyon-channel were converted into sediment dry mass (Mt) to allow for easier comparison with other global sediment fluxes. An average porosity of 60–80 % was assumed for the eroded sediment volume, and this porosity range was based on measurements from the upper 50 m of sediment at sites worldwide (Hay, 1998). An average density of sediment grains of 2.5 g/cm^3 is assumed, which is slightly less than the density (2.6 g/cm^3) of quartz grains, to account for less dense grains (e.g. ~2–3 % of organic matter). It is assumed that pore space is filled with seawater with a density of 1.035 g/cm^3. This implies a wet sediment density of 1.33–1.62 g/cm^3, and a dry sediment density of 0.5–1.0 g/cm^3. This is consistent with wet sediment density seen (1.1 to 1.6 g/cm^3) in cores through the upper few meters of sediment in the Congo lobe, whilst noting that sediment density will increase below those upper few meters below the seabed (Hay, 1998), and seafloor erosion often reached depths of 20–30 m (Figs. 5 and 6), and up to 50 m in the upper Congo Canyon.

3.3. Sediment cores

During the September–October 2019 cruise, seven piston cores were collected along the thalweg of the upper canyon, and three piston cores were collected along the thalweg of the deep-water channel. These piston cores had variable lengths of up to 9 m. Five sedimentary facies were identified and described via detailed sedimentary logs. The facies types observed in each core were then compared to the erosion depths at the core sites.

4. Results

4.1. Total volume of seabed erosion

A best estimate of 2.68 km^3 (and a minimum estimate of 1.00 km^3) of seabed sediment was eroded across the entire length of the Congo Canyon Submarine System between 2019 and 2020, as reported in Talling et al. (2022). However, the time-lapse surveys demonstrate that this erosion is not evenly distributed, and is often extremely localised.

4.2. Patterns of seabed erosion

A series of figures are used to illustrate patterns of seabed erosion, and much more minor deposition, for the survey area in the upper canyon (Fig. 5), and the survey area in the deep-sea channel (Figs. 6 and 7). These figures include plan-form maps showing distributions of erosion (in red) and deposition (in blue). A threshold of +/− 5 m for significant seabed change is used in the upper canyon (Fig. 4a), and a threshold of +/− 15 for the deep-sea channel that reflects the more conservative CUBE-based method for uncertainty estimation (Fig. 4b), below which colours are absent. These thresholds correspond to those where elevation changes likely exceed uncertainty estimates (Fig. 4). Figs. 5–7 also include plots illustrating depths of erosion (in red) or deposition (in blue), as measured along the canyon or channel axis transect. Changes in seabed gradient are also indicated along such transects. Finally, changes in the canyon's or channel's long profile from 2019 to 2020 are also shown, as measured along the canyon-channel axis, together with the position of ADCP moorings or cable breaks that document flow speed.

4.2.1. Patterns of erosion in the upper canyon

Erosion to depths of 10–20 m commonly occurs in the upper canyon between the 2019 and 2020 surveys, with erosion of up to 30–50 m in a few places (Fig. 5). But this erosion is localised, and unevenly distributed along the canyon, with intervening reaches of much more limited (<5 m) erosion. This patchy erosion is despite a relatively uniform flow front speed of ~5 m/s observed between mooring sites for the powerful January 14-16th turbidity current (Talling et al., 2022).

A ~0.09 km^3 landslide from the canyon flank occurred between 2005 and 2019 (at ~164 km in Fig. 5), which produces a substantial inflexion in the canyon's long-profile with a vertical height difference of ~150 m, called a 'knickpoint' (see Section 4.3.1). As described by Pope et al. (2022b), this landslide-dam also caused a wedge of sediment to accumulate for over 26 km upstream. This wedge of recent (post-2005 and pre-2019) sediment accumulation is up to 150 m thick, extends beyond the survey area, and has a volume of ~0.4 km^3 (Pope et al., 2022b). Fig. 5 demonstrates that reaches within ~4 km of the landslide dam are associated with deep erosion of >20 m. Erosional features produced by sidewall collapses also occur (see Section 4.3), only upstream of the landslide dam.

Zones of consistently deeper erosion occur along the upper canyon in the 2019–2020 difference map, including at the further upstream reach of the survey (140–155 km in Fig. 5a). Other zones of deeper (>15-20 m) erosion also occur, such as at the downstream reach of the survey area from 240 to 255 km (Fig. 5). However, intervening areas of much reduced erosion also occur along the canyon-axis, where depths of erosion are consistently below 5 m. Reaches of minimal erosion range from ~1 km to ~15 km in length (Fig. 5).

Zones of deposition that exceed the threshold of ~5 m for detection are much rarer. Deposits in the 2019–2020 difference map only have thicknesses of up to 5–10 m, and they occur over much shorter reaches (Fig. 5). These very limited depositional areas are mainly located on terraces in the upper canyon (Fig. 5).

4.2.2. Patterns of erosion in deep-sea submarine channel

The deep-sea channel has a more sinuous and deeper-incised upper part, and a straighter and less deeply incised lower part beyond a major avulsion at ~280 km in Fig. 7 (Picot et al., 2016, 2019; Talling et al., 2022). Erosion along the channel is also highly localised and patchy, with erosion depths commonly of 15–25 m, and occasionally up to 40 m (Figs. 6 and 7). In general, deeper erosion tends to occur more commonly and consistently in the channel's upper parts, including a zone from 45 to 65 km along the channel from the upstream start of the survey area in Fig. 6C. Erosion at channel bends is also better developed in this more sinuous upper channel reach from ~120–190 km along the surveyed channel (Fig. 6C). However, a zone of deep erosion also occurs from 210 to 230 km along the surveyed channel in deeper-water (Fig. 7a). This erosion is likely associated with up-slope migration of ~17 km by the head of a major knickpoint, although more detailed time-lapse surveys would be needed to be sure that old knickpoints have not been lost, and new ones created. But other zones of steeper channel gradients (i.e. knickpoints) in the distal part of the channel (>240 km from the start of surveyed channel) are not linked to major erosion (Fig. 7c-f).

4.3. Categories for types of seabed erosion

Erosion between 2019 and 2020 in the Congo Canyon and Channel has been divided into four categories (Figs. 8, 9), which are now

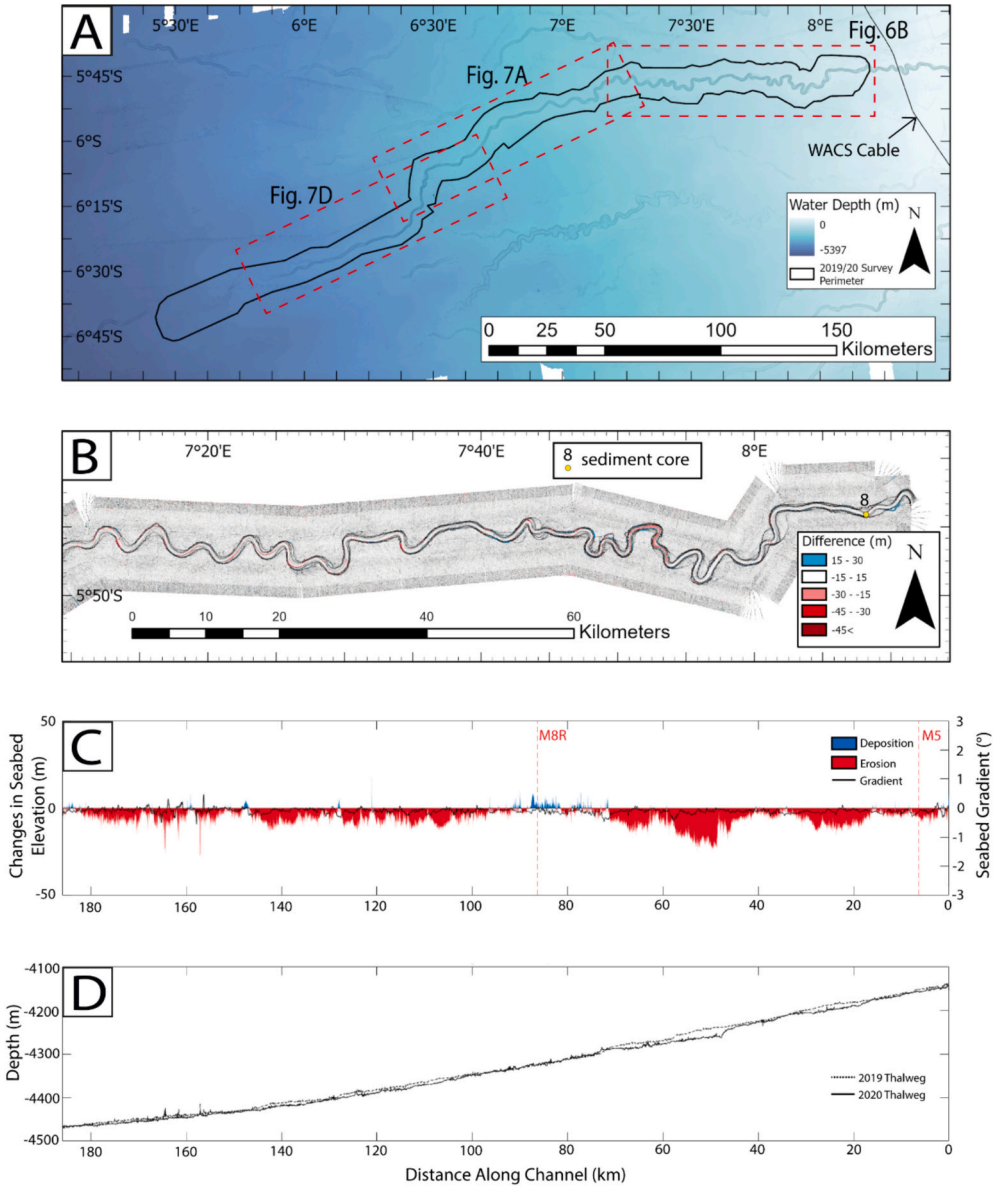

Fig. 6. A) Map of the Congo Submarine Channel showing the location of Panel B, Fig. 7A and D. B) Difference map showing changes in seabed elevation for the eastern (proximal) section of the deep-water channel, and core sites (yellow dots) (Figs. 11 and 12). C) Change in seabed elevation in a transect along the thalweg of the channel between September 2019 and September 2020, plotted with seabed gradient of thalweg. Mooring locations used to monitor turbidity currents are Indicated with vertical red dashed lines D) Long profile of the eastern channel thalweg in 2019 and 2020.

discussed in turn, with their key features summarised in Fig. 10. The total volumes of erosion have also been calculated for each of these categories, within the surveyed areas (Table 1).

4.3.1. *Knickpoints*

Knickpoints (Figs. 5-10a) are defined as anomalously steep steps in channel gradient, oriented across the channel, which migrate upstream via seafloor erosion (Gardner, 1984; Howard et al., 1994; Heiniö and Davies, 2007; Heijnen et al., 2020). In the Congo Canyon and Channel, we define any steep step in channel gradient (>7°) as a knickpoint, irrespective of whether the knickpoint migrated between 2019 and 2020. For comparison, the average gradient of the channel axis is between 0.1° and 0.5°.

If a knickpoint migrated between the 2019 and 2020 surveys, it created a zone of channel floor erosion between the older and newer knickpoint location, which has a relatively uniform depth of erosion in an across-channel or across-canyon direction (X-Y in Fig. 10a). Seven knickpoints were identified along the Congo Canyon-channel system (Fig. 8b, Fig. 9a). Of these seven knickpoints, 6 migrated between the 2019 and 2020 surveys, resulting in the removal of 0.24 km^3 [0.16 km^3] of canyon floor. However, the most distal knickpoint within the deepest-water part of the Congo Channel (i.e. from 240 to 300 km along surveyed channel in Fig. 7c) did not migrate.

4.3.2. *Outer bend erosion*

Outer bend erosion (Figs. 5–9) is defined as being focussed primarily on the outer bend of the canyon – channel floor. Discernible (<5 m in upper canyon and <15 m in deep-sea channel) erosion does not extend across the entire canyon-channel floor (Figs. 8c, 10c). This type of erosion accounts of 0.11 km^3 [0.02 km^3] of erosion throughout Congo Canyon-Channel, and it occurs within both the upper canyon (Figs. 5 and 8) and deep-sea channel (Figs. 6, 7 and 9). It is particularly well developed in the more sinuous part of the deep-sea channel (e.g. 120–180 km along surveyed channel in Fig. 6).

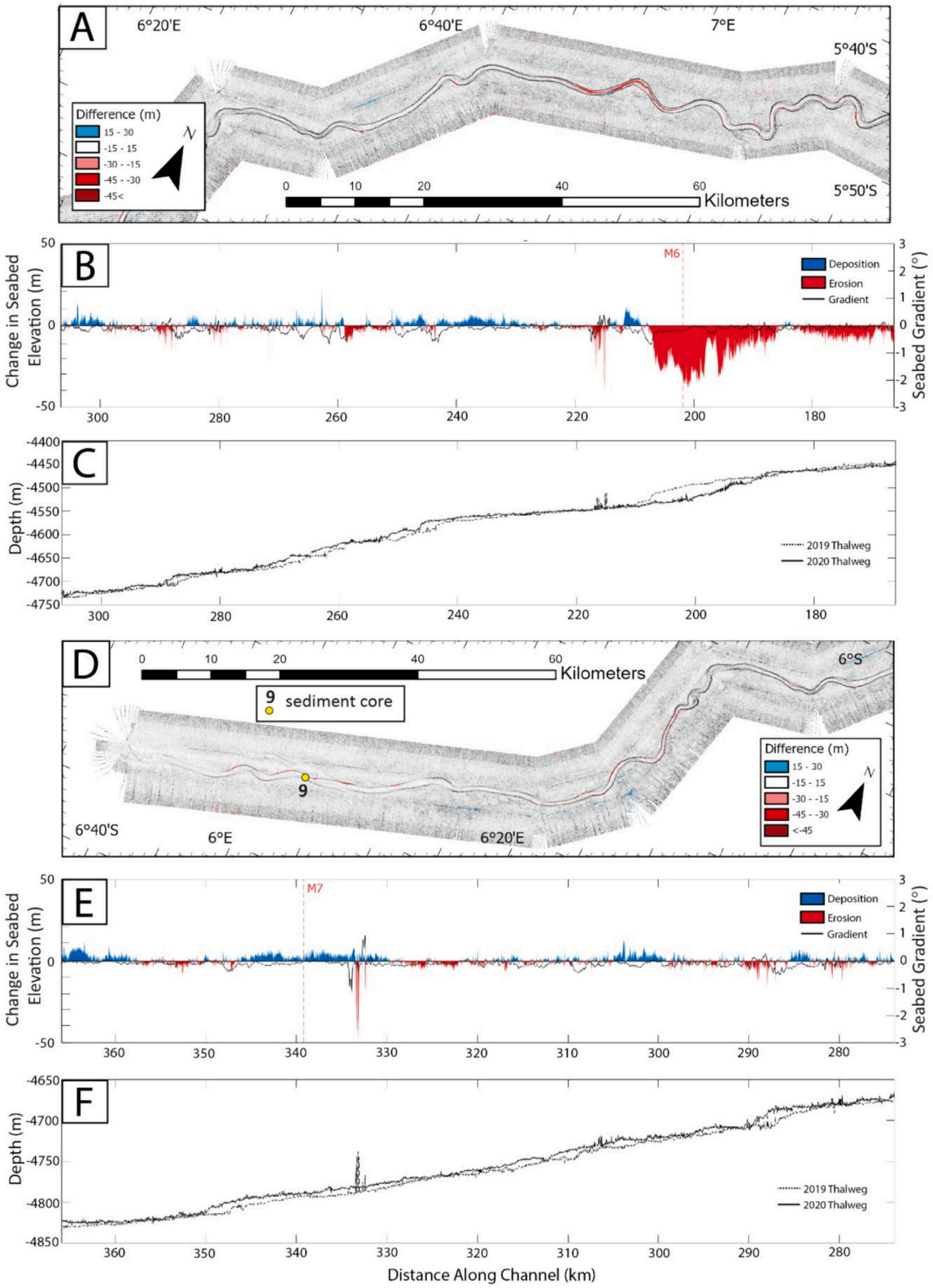

Fig. 7. A) Difference map showing seabed changes in the middle section of the deep-water channel (location shown in Fig. 6A). B) Change in seabed elevation in a transect along the thalweg of the middle part of the channel between September 2019 and September 2020, plotted with seabed gradient of thalweg. Mooring locations used to monitor turbidity currents are indicated with vertical red dashed lines. C) Long profile of the middle channel thalweg in 2019 and 2020. D) Difference map showing seabed changes in the western section of the deep-water channel (location shown in Fig. 6A). E) Change in seabed elevation in a transect along the thalweg of the channel between September 2019 and September 2020, plotted with gradient of thalweg. Mooring locations used to monitor turbidity currents are indicated with vertical red dashed lines F) Long profile of the western channel thalweg in 2019 and 2020.

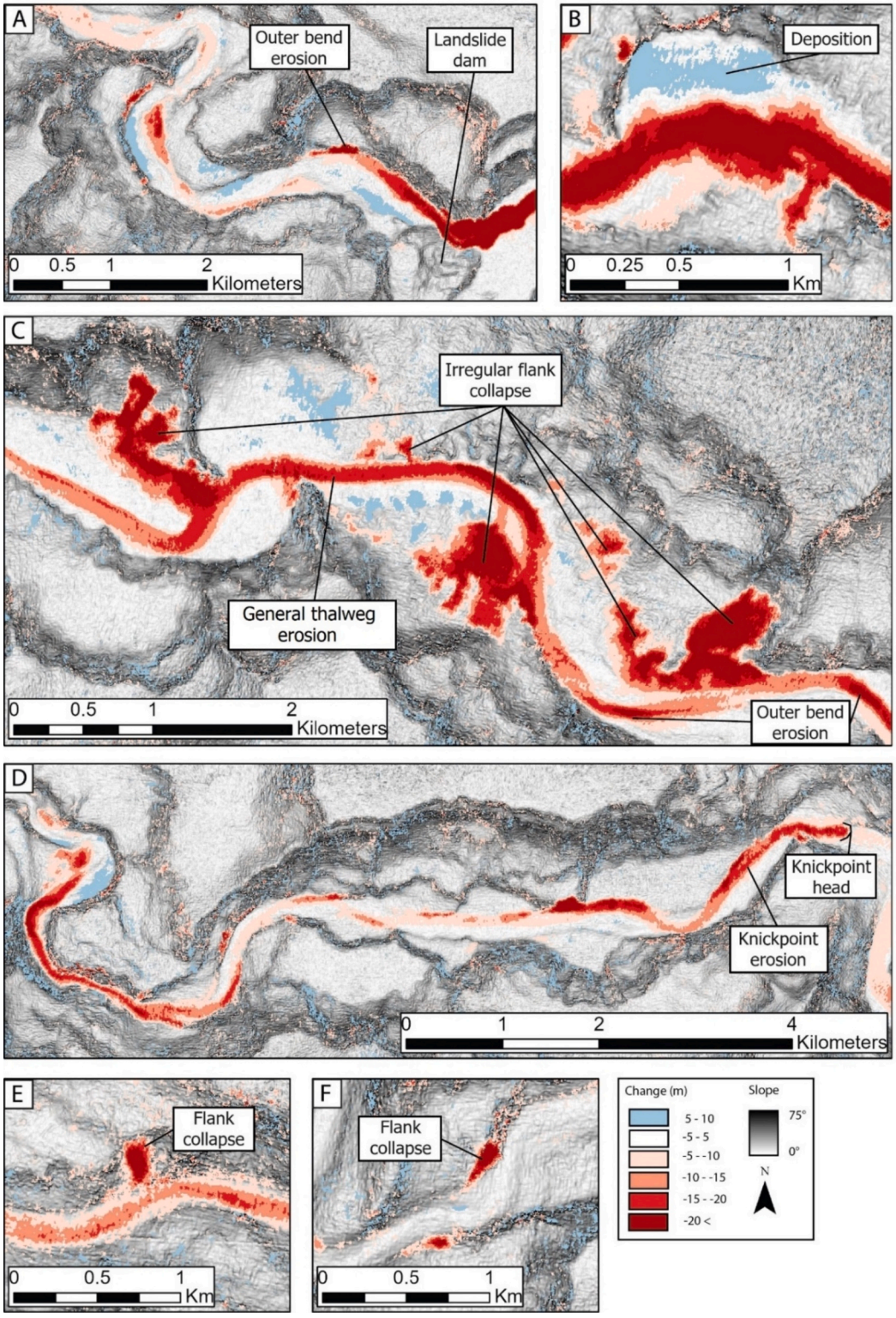

Fig. 8. Difference maps showing seabed changes (in metres) in the upper Congo Canyon between 2019 and 2020, with locations of each box shown in Fig. 1. The grey shaded base map shows seabed gradients in 2020. Shades of red correspond to areas of erosion, and blue to areas of deposition. Turbidity currents flowed from right to left. A) Seabed elevation change adjacent to the landslide dam reported in Pope et al. (2022b). Erosion occurs due to a knickpoint upstream of the landslide dam, with some deposition downstream of the landslide dam. Outer bend erosion is visible, resulting in bend amplification. B) Significant general thalweg erosion around a bend, with some deposition visible on the outside of the bend. C) Outer-bend erosion, general thalweg erosion and sidewall flank collapses. Note the lack of deposits associated with any sidewall flank collapses. D) Erosion due to knickpoint migration up canyon which also results in a straightening and widening of the canyon floor. E) Small sidewall flank collapse and general thalweg erosion. F) Sidewall flank collapse just before the apex of inner bends of the canyon, resulting in a 'straightening' of the channel floor.

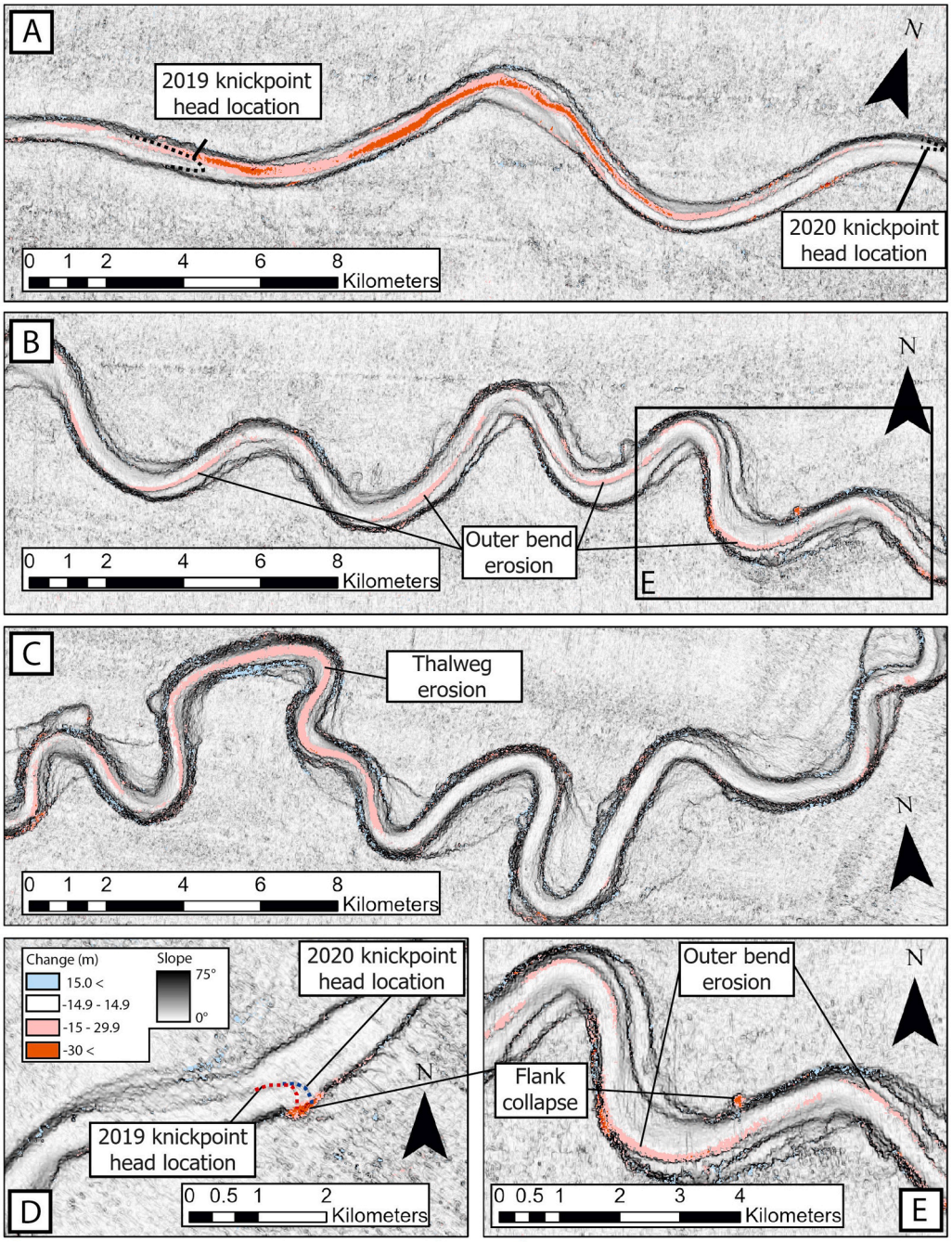

Fig. 9. Difference map of seabed change in the deep-sea channel between 2019 and 2020. The grey shaded base map shows seabed gradients in 2020. Shades of red correspond to areas of erosion, and blue to areas of deposition. Note there is limited deposition. Location of these detailed figures is shown by Fig. 1b. A) Knickpoint showing position of the knickpoint head in the 2019 and 2020 surveys, and associated erosion from knickpoint migration of 21 km. B) Outer bend erosion. C) General channel floor erosion to the west, and a lack of erosion to the east. D) A knickpoint at the end of the Congo Channel that migrated ~200 m up channel. The majority of this migration appears closely associated with a flank collapse. E) More detailed image of outer bend erosion on panel B. Note the small sidewall flank collapse on the inner bend.

The relative position of erosion on the outer bend is variable, when compared to the bend's apex. In the upper canyon (Figs. 5 and 8), this type of erosion occurs on the apex of bends, for sites downstream of the landslide dam. But it also occurs upstream of the bend-apex for sites located upstream of the landslide dam (Fig. 5A, C). In the deep-water channel, outer-bend erosion predominantly occurs just up-stream of the apex of a bend (Fig. 9B,E).

Outer bend erosion is visible in 15 % of bends, although this may be limited by the resolution of the bathymetry surveys. Some parts of the canyon-channel system have an entrenched thalweg (e.g. Fig. 7C). In this case, the outer bend erosion occurs on the outer bend of this entrenched thalweg, and not on the outer bend of the full width of the entire channel floor.

4.3.3. *General thalweg erosion*

General thalweg erosion is defined erosion occurring across the whole floor of the canyon or channel (Fig. 8b, Fig. 9c, Fig. 10b). It lacks a steep (>7°) section of seabed at its up-canyon limit, and associated sharp decrease in seabed erosion, and thus differs from a knickpoint (Fig. 10a). Unlike outer bend erosion, measurable (>5 m or >15 m) erosion occurs

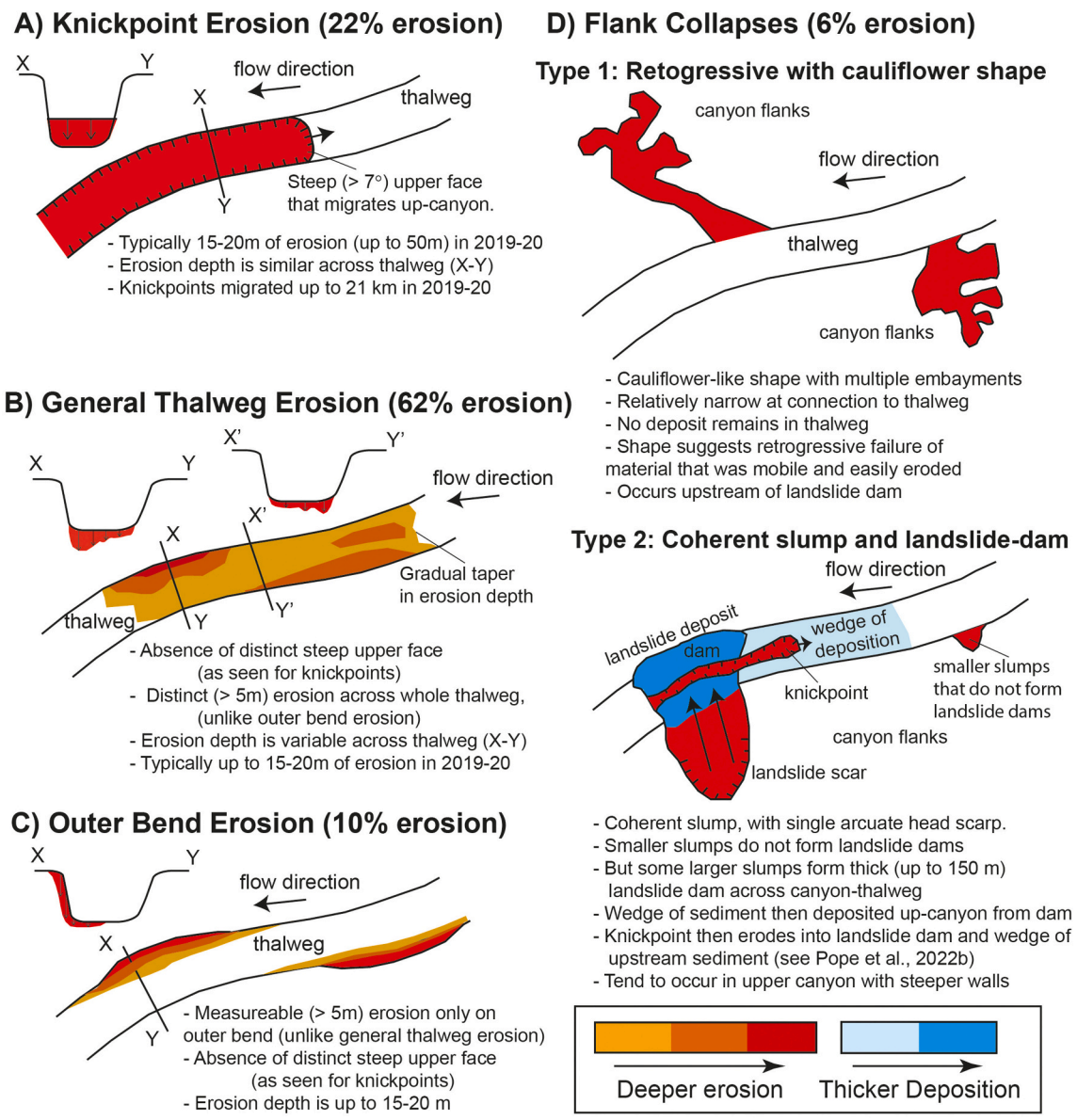

Fig. 10. Schematic summary of the categories for types of seabed erosion observed in the Congo Canyon-channel between 2019 and 2020, and their relative volumetric importance (Table 1). Red represents discernible erosion, and blue depicts measurable deposition in time lapse surveys. A) Knickpoint erosion. B) General thalweg erosion. C) Outer bend erosion. D) Two different types of sidewall flank collapses. See Pope et al. (2022b) for more details of landslide dams in the Congo Canyon.

across the whole canyon or channel floor, and is not restricted to just the outer bend (Fig. 10b,c). However, general thalweg erosion can display somewhat deeper erosion towards the outer bend (Fig. 10b), and we cannot confidently measure small amounts of erosion, which are <5 m in the upper canyon and <15 m in the deep sea channel. It is also possible that in some examples of outer bend erosion, erosion actually also occurred across the rest of the thalweg but was too shallow to measure. Thus, there may be a gradation between general thalweg erosion and outer bend erosion, at least in some cases, with general thalweg erosion being favoured by deeper erosion across a channel and greater resolution for the bathymetric data. It is also possible that our surveys lack enough vertical or lateral resolution to discern sufficiently small-scale and localised knickpoints.

General thalweg erosion accounts for 0.66 km^3 [>0.17 km^3] of the erosion in the Congo Canyon-channel, with such erosion being up to 47 m deep. Within the upper-canyon survey area (Fig. 1c), 82 % of the upper canyon floor is eroded by at least 5 m. In the deep-sea channel survey area (Fig. 1b), 67 % of the total channel floor is subject to erosion exceeding 15 m. In terms of total volume and extent, general thalweg erosion is substantially greater than erosion within the other categories (Table 1).

4.3.4. *Sidewall flank collapse*

Sidewall flank collapses (Figs. 8C,E,F and 9D,E) are defined as canyon-wall or channel-wall failures, and they differ from outer bend erosion (fig. 10c), as sidewall flank collapses do not erode the channel floor. There are two general types of sidewall failure (Fig. 10D). The first type of sidewall failure evacuated a cauliflower-shaped scarp that has multiple embayments, and material excavated from these embayments must past through a relatively narrow neck at the base of the landslide scar to reach the main channel-canyon axis (Figs. 8c, 10d). There are no deposits on the canyon-channel floor associated with these type 1 flank collapse (Figs. 8c, 10d). This geometry suggests that failure occurred retrogressively from the bottom up, and that failed material was highly

Table 1
Calculated volume of seabed change (km^3) and eroded sediment mass (Mt) between 2019 and 2020 in the Congo Submarine Canyon – Channel, divided into erosion categories, and into the two survey areas. Note: some total values may not be the sum of their parts due to rounding errors.

Erosion type and location	Volume of seafloor erosion (km^3)	Mass of sediment (Mt)	Normalised mass (Mt/km)
Change due to knickpoint migration			
Congo canyon	−0.09	−221.5	−2.0
Congo channel	−0.15	−384.6	−1.1
Total of both surveyed areas	−0.24	−606.0	−1.3
Change due to outer bend erosion			
Congo canyon	−0.01	−17.5	−0.2
Congo channel	−0.10	−260.2	−0.7
Total of both surveyed areas	−0.11	−277.7	−0.6
Change due to general thalweg erosion			
Congo canyon	−0.15	−375.0	−3.3
Congo channel	−0.51	−1274.1	−3.5
Total of both surveyed areas	−0.66	−1649.1	−3.4
Combined change due to knickpoints, outer bend erosion and general thalweg erosion			
Congo canyon	−0.25	−613.9	−5.5
Congo channel	−0.77	−1918.9	−5.2
Total of both surveyed areas	−1.01	−2532.8	−5.3
Change due to flank collapses			
Congo canyon	−0.05	−132.4	−1.2
Congo channel	−0.01	−29.9	−0.1
Total of both surveyed areas	−0.06	−162.3	−0.3
Total change			
Total erosion in survey areas	1.41	3528.9	7.4
Total deposition in survey areas	0.33	823.7	1.7
Net change in survey areas	−1.08	−2705.2	−5.6

mobile and easily eroded and entrained on the canyon-channel floor. Material comprising the landslide has presumably been reworked and carried further down-system, or transformed to a more mobile type of mass flow.

A second type of sidewall flank failure has previously been described in the upper Congo Canyon (Fig. 10d; Pope et al., 2022b). These are coherent slumps that have a single arcuate headscarp, and move as coherent blocks (Figs. 8e,f, and 9d,e). The majority of these flank collapses are small features that result in a local widening of the canyon or channel. In some extreme cases, the failed material can dam the main canyon-channel axis (Fig. 10d; Pope et al., 2022b). These landslide-dams are much less easily eroded than material from type 1 cauliflower-shaped flank failures. However, in the type 2 sidewall flank failure described by Pope et al. (2022b), a relatively deep knickpoint progressively incises the landslide dam, and then migrates upslope through a wedge of sediment previously deposited due to the landslide dam (Fig. 8a; Fig. 10d; Pope et al., 2022b).

Sidewall flank collapses of both types accounted for 0.06 km^3 [>0.05 km^3] of eroded material, which equates to ~6 % of the total erosion in between the 2019 and 2020 surveys (Table 1). There are 51 flank collapses within the upper canyon survey area, with the largest examples having a (type 1) cauliform shape (e.g. Figs. 5,8c). There are 24 discernible sidewall flank collapses within the deep-water channel that tend to have a single arcuate headscarp (type 2), although they did not create landslide-dams (Figs. 7, 9).

4.4. Volumes of seabed erosion and deposition

Volumes of seabed erosion (km^3) and their equivalent mass (Mt) are provided for surveyed areas in Table 1, along with normalised mass (Mt) per km of canyon-channel floor to allow for easier comparison between erosional processes. This normalised mass is calculated by dividing the total mass eroded within the survey area by the total sinuous length of the thalweg within the survey. Table 1 is divided into the following types of erosion (i) knickpoints, (ii) outer bend erosion, (iii) general thalweg erosion and finally (iv) sidewall flank collapse, as described above. The volumes of sediment eroded are shown for the upper-canyon and deep-sea channel survey areas (Fig. 1), as well as for each category of erosion.

Table 1 only includes volumes of erosion in the surveyed areas from 2019 to 2020, which account for 40 % of the total length of the Congo Canyon-Channel. Volumes of erosion for the entire length of the system are then estimated. This is done by assuming the remaining 60 % of the canyon-channel follows a similar pattern of erosion, with the same fraction of different categories of erosion. This assumption may be somewhat biased, as the deep-water channel forms a relative high fraction of the 40 % of the system that was surveyed, with only a shorter reached surveyed in the upper canyon (Fig. 1). However, this assumption is necessitated by a lack of surveys in intervening parts of the system.

General thalweg erosion accounts for 62 % of the total erosion from 2019 to 2020, knickpoints account for 22 % of erosion, outer bends for 10 % of erosion, and sidewall flank collapse for 6 % of erosion. General thalweg erosion, knickpoint erosion and outer bend erosion all occur on the canyon's or channel's floor, and when combined they contribute 94 % of all erosion in the canyon-channel from 2019 to 2020.

4.5. Sediment cores

Sediment cores from the thalweg of the upper canyon (Figs. 5 and 12) comprise five facies types (Fig. 11; and see Baker et al., 2024). The most common facies type (47 % of the cores) in the cores is homogeneous or bioturbated clay (Fig. 11). Homogeneous or bioturbated silt facies makes up 22 % of the cores and contains occasional laminations or normal grading to clay. The muddy sand facies (18 % of the cores) comprises mud with fine- to medium-grained sand, that may be ungraded or normally graded and contain mud, sand or vegetation-rich muddy-sand clasts. Massive, clean, fine- to medium-grained sand comprise only 9 % of the cores, contains rare mud or muddy-sand clasts, and is often ungraded or occasionally normally graded (Fig. 11). Finally, vegetation-rich muddy sand facies comprises 4 % of the cores and contains concentrated, well-preserved mm- to cm-sized black wood and plant debris within a fine-grained sand-mud matrix with no grading (Fig. 11). Six of the seven cores are dominated by facies with a high cohesive mud component, albeit with muddy sands and interbedded thin clean-sands (Fig. 11), and these cores are 2.5 to 9 m in length. One shorter (1.3 m long) core contained remobilised clean sand that appeared to have been sucked-in during coring, and thus may not represent the near-surface seabed properties at this location (Fig. 11). Additional sediment cores collected in 2019 from terraces at heights of 50 to 300 m above the thalweg contained thin-bedded (<5 cm) turbidites, with alternations of thinly bedded silt and clay facies.

The sediment composition of the thalweg of the Congo deep-water channel is poorly constrained by two sediment cores collected in 2019 (Fig. 12; core locations in Figs. 6 and 7) and four cores described in the published literature (cores KZAI-06, KZAI-15, KZR-19 and KZR-21; Babonneau et al., 2010; Baudin et al., 2010; Migeon et al., 2004). These channel-floor cores ranged from 2 to 7 m in length and primarily contained massive, often ungraded, clean sands with occasional clasts of plant debris or mud (Fig. 12; Baudin et al., 2010 their Fig. 3; Babonneau et al., 2010 their Fig. 7). Two of the cores contained silt and clay facies in

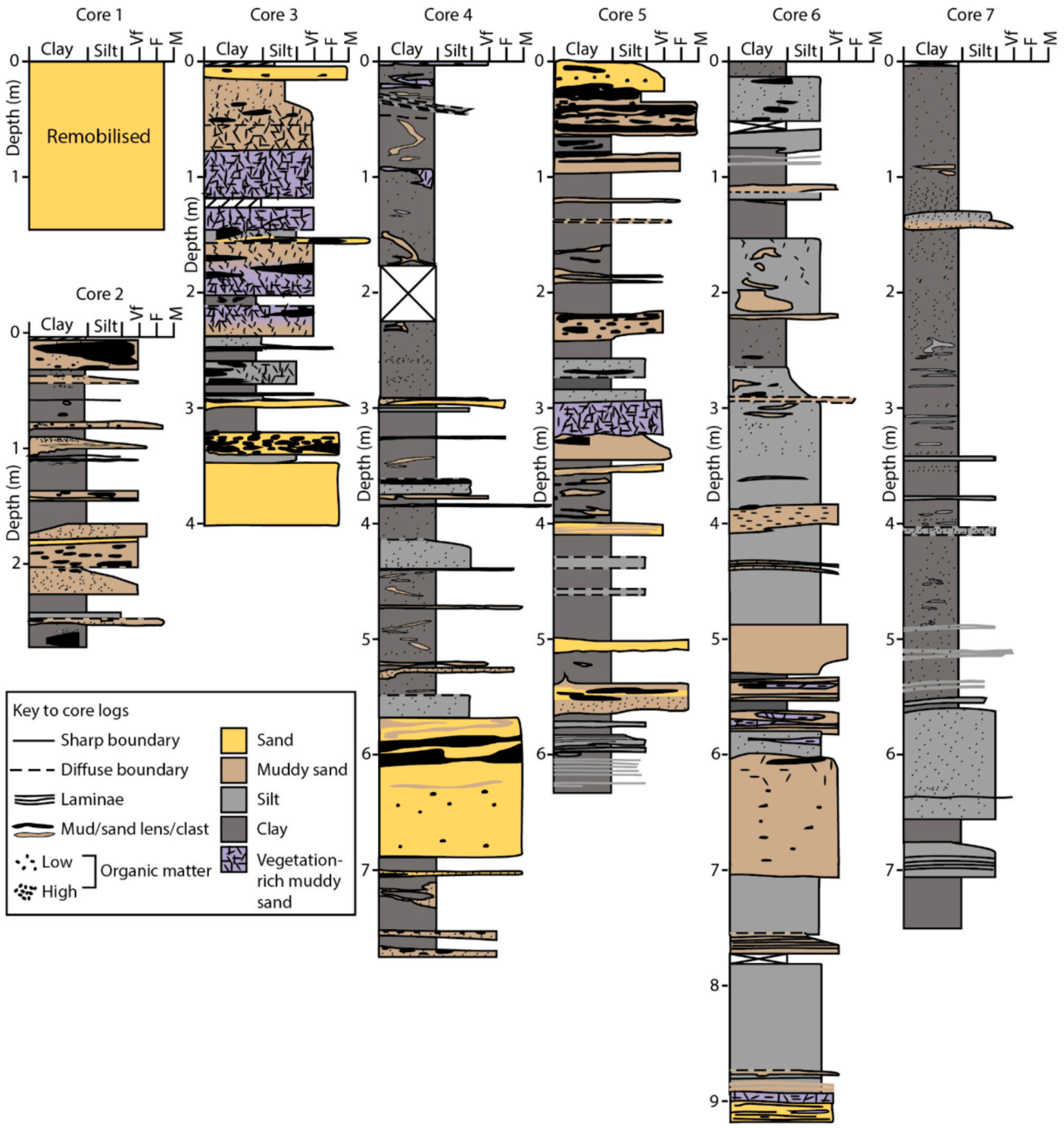

Fig. 11. Sedimentary logs of cores in the upper canyon collected in 2019 (adapted from Baker et al., 2024). See Fig. 5 for core locations, and Fig. 12 for patterns of erosion in 2019–2020 in areas adjacent to these core sites.

the top 0.2 m (KZAI-06; Baudin et al., 2010) and the top 1 m (Core 8, this study). These cores thus suggest the main channel is dominated by sand.

5. Discussion

This paper presents time-lapse surveys of a major submarine canyon-channel, which capture how powerful (up to 5–8 m/s) and extremely long (>1100 km) runout turbidity currents modify the seabed. Understanding interactions between turbidity currents and the seabed is important for several reasons. First, it helps to understand how powerful and long runout turbidity currents sustain themselves for >1100 km, eroding the seafloor to maintain or increase their density. Second, it helps to understand where optimum locations may be for submarine telecommunication cables, or other seabed infrastructure, to survive the effects of powerful turbidity currents. Third, it helps to understand residence times of sediment and organic carbon within a submarine canyon-channel, which is important for global sediment and carbon budgets. Finally, insight into processes and volumes of erosion can help to improve future numerical models of canyon flushing turbidity currents.

5.1. Patterns and processes of seabed erosion

Our first objective was to understand how canyon flushing turbidity currents interact with the seabed, and the resulting patterns and processes of seabed change.

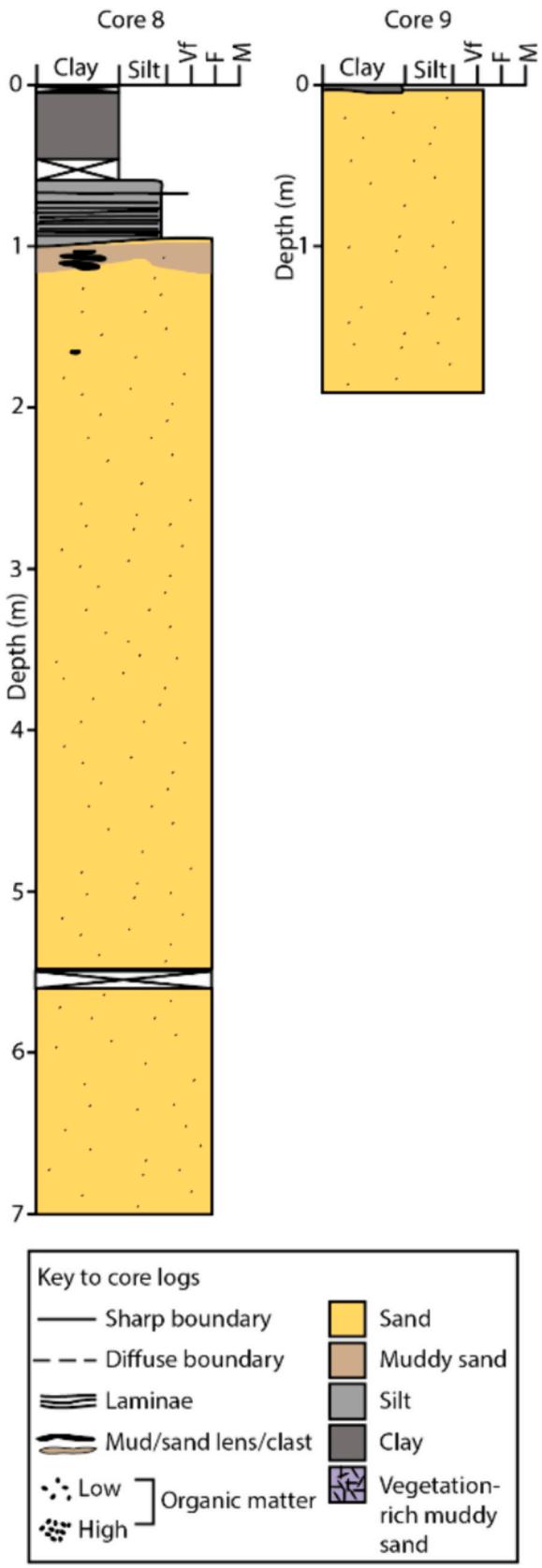

Fig. 12. Sedimentary logs of cores in the deep-sea channel collected in 2019, whose location is shown by Figs. 6 and 7. These sand-dominated cores are similar to four other cores from the floor of the deep-sea channel described by Babonneau et al. (2002, 2010).

5.1.1. Erosion dominates over deposition

Erosion is the dominant process, volumetrically accounting for ~80 % of observed seabed change (Table 1). The axis of this submarine canyon-channel was dominated by erosion and bypass of sediment rather than deposition, even in the current global high stand in sea-level. This observation from the modern Congo Canyon emphasises the importance of bypass surfaces (Stevenson et al., 2015) within ancient canyon-channel deposits, and that bypass surfaces can represent composite erosion events, and be highly time transgressive.

Depths of erosion of 15–20 m are relatively common in both the canyon and channel, with maximum erosion depths of up to 50 m (Figs. 5–7). This dominance of erosion may reflect the sustained velocities (>5–8 m/s) and power of the two canyon flushing turbidity currents, which occurred on January 14-16th 2020 and March 8th 2020 (Fig. 2; Talling et al., 2022). However, due to the relatively short lengths (<10 m) of available sediment cores (Figs. 11 and 12), and poor quality and penetration of sub-bottom profiler data along the canyon-channel axis, it is not clear whether this depth of erosion is sufficient to incise underlying bedrock or whether it only removes previous canyon-channel fill deposits.

Sediment deposition accounts for only ~20 % of mapped seabed change (Table 1) across smaller areas of the canyon-channel system, with deposit thicknesses only occasionally reaching 5–8 m (Figs. 5–9). However, it should also be noted that these time lapse surveys are only able to unambiguously resolve deposits that are thicker than ~5 m in the upper canyon, and ~15 m in the deep-sea channel. Thus, more extensive but thinner areas of deposition may occur, including on external levees or internal terraces which our surveys would not resolve. A tendency for deposits to be thinner than the eroded depths could also contribute to an imbalance between observed volumes of erosion and deposition (Table 1).

5.1.2. Erosion is highly localised and patchy

A striking observation is that deep (>15–20 m) seabed erosion is highly localised and patchy, with deeply eroded reaches alternating with reaches of much more limited erosion (Figs. 5–7). This strong localisation of erosion occurs despite monitored flow front speeds that maintain relatively constant speeds of 5–8 m/s, at least on long length scales between moorings or cables (Fig. 2b). Although we lack more finely resolved information on flow speed between mooring sites or cable-breaks (Talling et al., 2022), it seems unlikely that strong fluctuations in the depths of erosion are due to relatively rapid fluctuations in overall flow speed, often over downstream distances of just a few kilometers in the canyon (Figs. 5 to 7). Indeed, the fastest flow front speeds in the most powerful January 14-16th turbidity current occurred close to the end of the deep-sea channel (Fig. 2a; Talling et al., 2022), along a reach where there was relatively little erosion (Fig. 7D-F). Thus, it is unlikely that fluctuations in overall (i.e. over >10–100 km) flow speed drive this patchy erosion, which must presumably be due to other processes.

5.1.3. Cored substrate types and patterns of seabed erosion

It could be proposed that localised changes in seabed sediment properties may cause the observed patchy seabed erosion. A limited number of widely spaced sediment cores from the thalweg of the upper canyon were collected in 2019 (Fig. 11). More numerous and closely spaced cores would be needed to document local variations in seabed sediment facies, or indeed how facies vary across localised features such as knickpoints. Moreover, these cores penetrated to depths of <9 m, and thus only capture the upper parts of the stratigraphy eroded between 2019 and 2020 (Fig. 11). However, given these caveats, there is no clear correlation between the facies in these sediment cores and depths of nearby erosion along the thalweg (Fig. 13).

The dominance of muddy facies in the upper canyon cores, at least in the upper parts of the stratigraphy (Fig. 11), suggests that erosion processes must be able to excavate cohesive material, and erosion is thus not

restricted to grain-by-grain detachment or liquefaction of coarser and less cohesive sands.

In contrast, the small number of cores from the axis of the deep-sea channel collected in 2019 (Fig. 12), and by the previous study of Babonneau et al. (2010), are dominated by clean sand facies. Again, there are few cores available, and these cores are insufficient to test robustly whether changes in seabed sediment types are linked to localised erosion (Fig. 12). However, sediment eroded in 2019–2020 in the deep-sea channel likely has a higher sand component. This higher sand content could potentially allow additional erosional processes to occur, such as erosion via wholesale liquefaction of loosely packed clean-sand or breaching of more tightly packed clean-sand.

5.1.4. Localised erosion due to pre-existing topography

It appears that variations in seabed sediment properties may not explain completely the observed localised and patchy nature of seabed erosion during the canyon flushing flows in 2019–2020, although more closely spaced cores would be needed to test this hypothesis fully. Thus, another explanation of the patchy erosion may be needed. It is thus proposed here that pre-existing topographic features, such as knickpoints, may also play a key role in producing localised erosion. Once these topographic features develop, they then play a key role in causing further localised erosion (see Section 5.2.1 below).

5.2. Processes of seabed erosion and their volumetric importance

Processes of erosion listed in Table 1 are now discussed in more detail to better understand how they operate, and what controls their spatial distribution along the canyon-channel system.

5.2.1. Knickpoint erosion

Knickpoints play a significant role in seabed erosion, and account for 22 % of total erosion observed between the 2019 and 2020 surveys (Fig. 10a; Table 1). They may play an important role in generating patchy and localised seabed erosion along the floor of the canyon-channel, as seen elsewhere (Heijnen et al., 2020). By far the largest (~150 m high) knickpoint in the Congo Canyon was generated between 2005 and 2019 by a side-wall collapse (Fig. 5; Pope et al., 2022b), but various other smaller (<20 m high) knickpoints occur along the system (Figs. 5–7). A total of seven knickpoints were mapped, but only six of

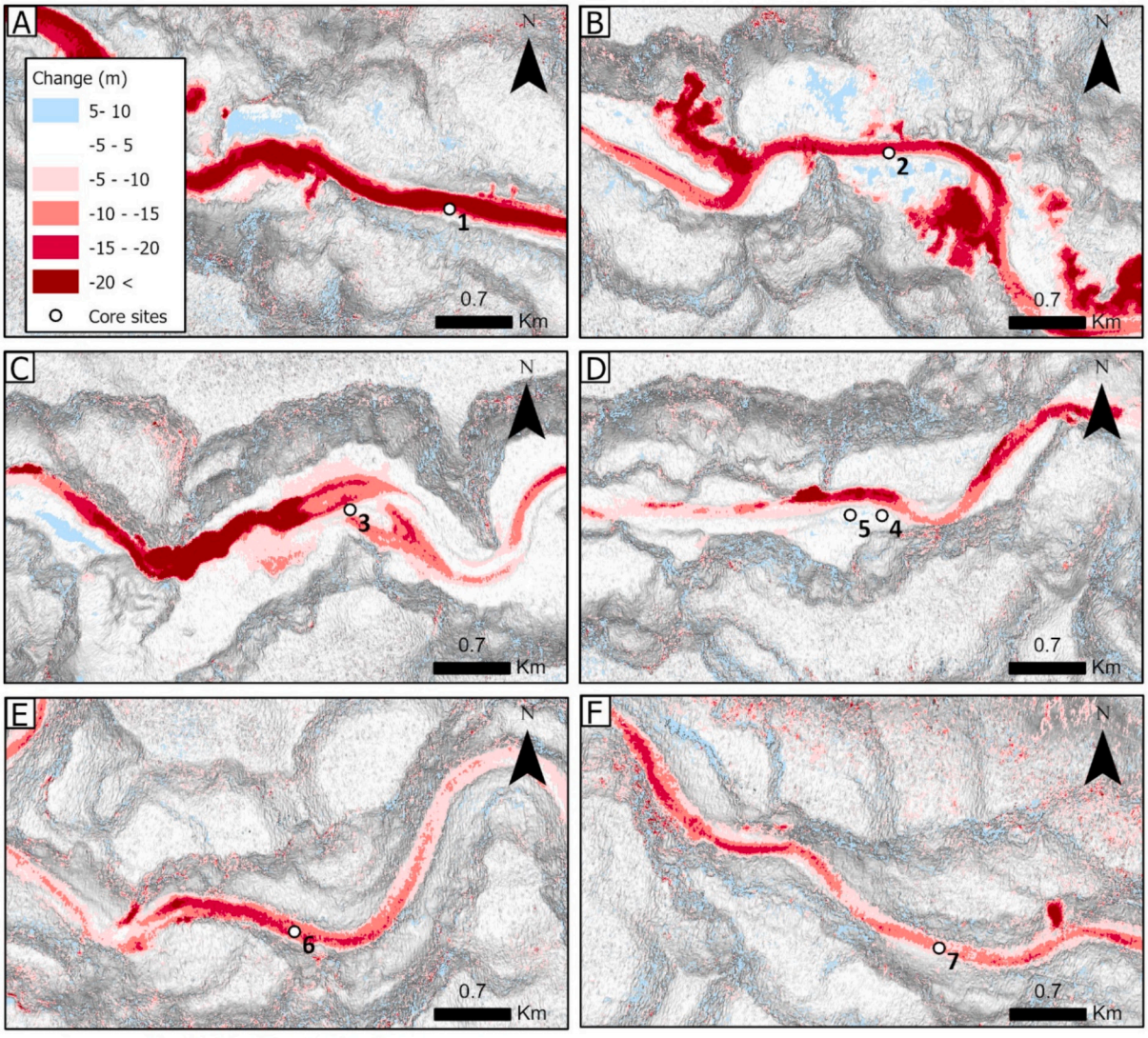

Fig. 13. Maps showing location of piston cores collected in 2019 in the upper canyon, and depths of erosion and deposition within the surrounding areas from 2019 to 2020. Detailed sedimentary logs of these cores are shown in Fig. 11, and Fig. 5 provides an overview map of their broader positions along the upper canyon. (A) Core 1. (B) Core 2. (C) Core 3. (D) Cores 4 and 5. (E) Core 6. (F) Core 7. Each map comprises seabed gradients (grey shade) and erosion-deposition depths (red-blue colours).

these knickpoints migrated measurably during the 2019–2020 study period at the resolution of our bathymetric surveys. One of these knickpoints (at 190–210 km in Fig. 7A-C) migrated 21 km upstream in a single year, which is by far the fastest submarine knickpoint migration rate yet recorded. Monitoring at other sites suggests knickpoints are common in submarine canyons or channels, but migration rates were on average 50–200 m/year, and up to 450 m/year (Heijnen et al., 2020, 2022). The far higher rate of migration for this knickpoint in the Congo Channel may reflect the more prolonged duration and high speeds of the turbidity currents it experienced.

However, it is also striking that one large knickpoint zone (240–290 km in Fig. 7) did not move significantly from 2019 to 2020, whilst being located ~130 km downflow of the knickpoint that migrated 21 km. This is despite the deepest water part of the channel experiencing the highest (8 m/s) turbidity current front speeds (Fig. 2b; Talling et al., 2022). This example suggests that additional factors, beyond powerful (i.e. 8 m/s) flow speed, affect knickpoint migration rates. In general, the distal part of the channel displays limited erosion (Fig. 7D-F), and this might be linked to the distal channel's shallower depth and lower sidewall heights, and likely greater overspill and dissipation of turbidity currents (Talling et al., 2022). But it may also suggest that localised seabed substrate properties could also strongly affect knickpoint migration, although available cores in the deep-sea channel are too widely spaced to test this hypothesis (Fig. 12). This observation that not all knickpoints migrate may be important if cable routes are chosen to avoid knickpoints, under an incorrect assumption that all knickpoints migrate during canyon-flushing flows.

These time lapse surveys also appear to capture the initiation of a new knickpoint in the channel (at 45–70 km in Fig. 6) between 2019 and 2020. However, erosion patterns and migration of individual knickpoints can be complex. Further research is needed to better understand what controls the origin, migration pattern and rate, and eventual termination or flattening of submarine knickpoints.

5.2.2. General thalweg erosion

Although knickpoints cause significant (22 %) erosion, a much greater percentage (62 %) of the total erosion is focussed along the channel or canyon floor, at sites where knickpoints (with distinct headwalls at their upstream end) are not observed at the resolution of these surveys (Fig. 10B). This category of general thalweg erosion is responsible for the largest volumes of erosion, and it lacks obvious steepening that characterises knickpoints (Fig. 10A). It therefore appears localised and patchy seabed erosion may often occur without an obvious steeping or knickpoint. This in turn suggests local factors other than increased gradients can lead to patchy erosion, perhaps including variable substrate properties. More closely spaced and detailed cores would again be needed to test such links to substrate properties.

5.2.3. Outer bend erosion

Outer bend erosion occurs throughout both the Congo Canyon and Channel (Fig. 10C), and it accounts for 10 % of total erosion (Table 1). Outer bend erosion can occur before, at, and after the apex of a bend (Figs. 8 and 9). This is a surprising finding, as it is expected to find erosion at the apex of the bend in accordance with the results of Palm et al. (2021). Finding outer bend erosion at such variable positions around a bend suggests that there are knowledge gaps in understanding of these flow process and bend dynamics.

5.2.4. Sidewall flank collapse erosion

Cauliflower-like (type 1; Fig. 10d) sidewall failures occurred between 2019 and 2020 in both the Congo Canyon and Channel, but they occurred more frequently within the more proximal canyon (Fig. 4). Previously, a large coherent slump (type 2) occurred in the upper canyon (Figs. 5 and 10d; Pope et al., 2022b). This greater frequency of flank collapses is most likely due to canyon walls that are larger in this upper reach, where they are ~400–450 m above the thalweg in the surveyed areas of the canyon, compared to 0–150 m above thalweg in the surveyed areas of the channel. It is also likely due to a higher frequency of turbidity currents (Fig. 2; Azpiroz-Zabala et al., 2017; Simmons et al., 2020; Talling et al., 2022) in the upper canyon and the undercutting of the sidewalls that results. Smaller sidewall failures with single arcuate headscarps, which did not form landslide dams, also occurred in 2019–2020 on the flanks of the upper canyon (Fig. 8E,F) and deep-water channel (Fig. 9D,E).

The location of unusually large and frequent type 1 flank collapses in the reach upstream of the previously identified landslide dam (Figs. 5, and 8C) suggests a causal relationship. It could be possible that these type 1 failures initiated within the 100 m thick wedge of rapidly deposited (and thus poorly consolidated) sediment that accumulated upstream of the dam and thus retrogressively failed up the canyon walls (Pope et al., 2022b). This rapidly deposited sediment may also have excess pore pressures which could destabilise the sediment through dewatering, thus making it more prone to erosion. Furthermore, some type 2 flank collapses occurred on the inner bends (Figs. 8F, 9E) where small sections of canyon-channel wall were protruding. These collapses result in a ‘straightening’ of the channel due to flushing turbidity currents.

5.2.5. Dominance of erosion along canyon or channel floors

Three of these processes (knickpoint migration, outer-bend erosion, and general thalweg erosion) effect the channel or canyon floor, and when combined these categories account for 94 % of the total eroded volume (Fig. 10; Table 1). A general predominance of erosion across the floor of the canyon or channel may be expected for several reasons. Most importantly, the canyon or channel floor experiences the highest bed shear stresses, sometimes for prolonged periods, which in turn favour increased erosion. It is also possible that channel-floor sediment is less consolidated than sediment on adjacent canyon or channel-flanks. Focussed erosion along the canyon's or channel's floor may also favour development of dense near-bed layers, of the type inferred from flow monitoring in the upper Congo Canyon (Azpiroz-Zabala et al., 2017) or elsewhere (Hughes Clarke, 2016; Normandeau et al., 2020; Paull et al., 2011, 2013, 2018; Pope et al., 2022a; Talling et al., 2023). Such dense near-bed layers, which are restricted to the canyon-channel floor, may themselves be powerful agents of erosion. It is perhaps more surprising that erosion along the canyon-channel floor is so highly localised and patchy, given that bed shear stresses, differences with flank sediment, and presence of dense near-bed layers might be expected to act in a more uniform fashion along the canyon-channel system.

5.3. What controls the occurrence and distribution of different erosional processes?

Our third objective is to understand the spatial distribution of erosion. Previous sections have summarised how landslide dams may both initiate large knickpoints (Pope et al., 2022b), and favour side wall collapses that originate in recently and rapidly deposited sediment wedges upstream of these landslides. In addition, the most distal reach of the submarine channel has limited erosion (Fig. 7), despite experiencing the fastest flow front speeds in the January 2020 turbidity current (Fig. 2). It is also apparent that outer bend erosion is only well developed along certain reaches, such as the sinuous section from 120 to 190 km (Fig. 6) along the deep-sea channel.

Here we present a hypothesis that may help to explain the long-profile evolution of canyon channel systems, and also explain why erosion is often localised and patchy. Based on observed changes in the channel long profile between 2019 and 2020, it is proposed here that the long-profile locally tends towards an equilibrium profile, as also described in Guiastrennec-Faugas et al. (2020) in the Capbreton Canyon. Long stretches of the Congo Canyon-channel system have near-uniform gradient, such as within the upper-canyon, which has a gradient between 0.57° and 0.17° (Fig. 5c). Seabed erosion, including via migration

of knickpoints, tends to remove material located above this equilibrium long profile (Fig. 5c). Conversely, reaches of the canyon or channel floor that lie along the equilibrium profile undergo much less erosion (e.g. from 290 to 350 km along the surveyed channel in Fig. 7). This preferential erosion for sites above the equilibrium profile results in linear long profile that has a near-uniform gradient, and it may produce localised and patchy erosion.

Long profiles with near uniform gradients also occur in other submarine canyons, suggesting this may be a more general process, despite differences in canyon margin type (e.g. Guiastrennec-Faugas et al., 2020). For example, the profile of Monterey Canyon has a uniform gradient, except where it is disturbed by the Navy Slump (Paull et al., 2011), whilst the long profile of La Jolla Canyon is also very linear (Paull et al., 2013).

5.4. Wider Implications

We now summarise the wider implications for hazards to seabed cables, turbidity current modelling and interpreting ancient canyon-channel systems in the rock record. The observed patterns of often highly localised and deep (>10–40 m) erosion will also have significant implication for seabed life (Bigham et al., 2023), which may be locally scoured away in such events. These erosion patterns will also have implications for how previously deposited sediment, and the organic carbon it contains is remobilised and transferred to the deep sea in multiple stages (Hage et al., 2020, 2022, 2024; Baker et al., 2024; Talling et al., 2024).

5.4.1. Assessing and mitigating hazards to cables

This study shows that seabed erosion is very patchy, with localised areas of deep erosion, and intervening reaches of little erosion. Previous work has shown how submarine cables may be badly damaged or broken by powerful canyon-flushing turbidity currents (e.g. Talling et al., 2022; and also Heezen and Ewing, 1952, Carter et al., 2014 and others). However, a surprising observation in the Congo Canyon was that although the January 14–16th 2020 flow broke three cables, an intervening cable survived (Fig. 2a; Talling et al., 2022). This implies that some local conditions are favourable for seabed cables surviving such powerful flows, whilst other locations are not, presumably including areas of especially deep (>10 to 50 m) seabed erosion. It is therefore suggested that seabed telecommunication cable routes should avoid areas that are prone to deeper erosion, such as locations that are upslope from landslide dams, near knickpoints, and immediately after bend apices.

Thus, it will be highly advantageous to survey a canyon-channel floor before cables or other seabed infrastructure are deployed, to locate the positions of knickpoints and landslide dams. Ideally, repeat time-lapse surveys should be collected that also determine the rates of up-canyon knickpoint migration. The cables or other seabed infrastructure should avoid both the current position of knickpoints, but also areas upstream of a knickpoint that could be affected by its future migration. The infrastructure should also try to avoid regions of the canyon floor above an equilibrium profile, as these areas may also be prone to greater erosion (Section 5.3), even if there is no steepening from an identified knickpoint.

5.4.2. Modelling turbidity currents

Previous work has shown that turbidity current behaviour is critically dependent on the exchange of sediment with the seabed (i.e. erosion and deposition). For example, seabed erosion may cause a turbidity current to become denser and faster, and thus lead to more erosion; a process termed ignition (Parker, 1982). Indeed, modelling by Traer et al. (2012) suggested that processes of bed erosion may dominate the first order behaviour of turbidity currents. This is confirmed by previous numerical modelling of turbidity currents in the Congo Canyon by van Rijn et al. (2019), although that modelling produced unrealistic continuous increases in flow speeds (via ignition) from 0 to 9–17 m/s (cf. Fig. 2). Thus, erosional processes are as yet poorly constrained, and highly challenging or impossible to reproduce in laboratory flume experiments due to scaling issues (Talling et al., 2023).

It is indeed clear that seabed erosion can substantially increase the volume of sediment carried by turbidity currents (i.e. bulk up), with the volume of sediment eroded by the 2019–2020 canyon flushing flows in the Congo Canyon being 20–50 times the annual sediment supply from the Congo River (Talling et al., 2022). In addition, Pope et al. (2022a) showed that turbidity currents in Bute Inlet cumulatively bulked up by a factor of 10 by the mid-fjord. Thus, the amount of sediment eroded from the seabed can exceed the amount of sediment initially carried by the flows by an order of magnitude or more. However, such pronounced bulking only results in rather small increases in flow front speeds, and highly erosive flows can sustain similar flow speeds over long distances, contrary to ignition theory. This has led to an alternative 'travelling' wave model where sediment supplied via basal erosion into the fast and dense frontal part of the flow, is near-balanced by sediment shed from the frontal zone into trailing body and tail; thus allowing highly erosive flows to have constant front speeds (Heerema et al., 2020; Talling et al., 2022, 2023).

This contribution seeks to better constrain processes by which seabed erosion occurred in the Congo Canyon, although we lack detailed direct measurements from the base of active flows, which will continue to be very challenging to acquire. However, some important conclusions can still be drawn.

Erosion in the Congo Canyon was often relatively deep (15–20 m), and there will be order of magnitude or more increase in sediment shear strength with depth due to compaction and other processes in the upper 20 m of sediment, with the greatest changes in shear strength occurring in the upper few meters of sediment (e.g. Sawyer and Devore, 2015). Thus progressive changes in sediment shear strength may need to be accounted for within numerical models of seabed erosion.

Here we emphasise that erosion of the seabed is also highly localised and patchy over distances of a few kilometers or less, even though the front speed of the turbidity currents was relatively uniform over long distances of >50–100 km (Fig. 2; Talling et al., 2022). Localised erosion is also not fully explained by variations in seabed sediment type, as mud-dominated cores in the upper canyon come from sites that later underwent variable depths of erosion (Figs. 12 and 13). Erosion of outer bends occurs, but other types of erosion are volumetrically more important (Table 1), and significant erosion can characterise straighter as well as sinuous segments of the canyon-channel course. Thus, a sinuous course of the canyon-channel, and resulting higher bed shear stresses at outer bends, cannot fully explain such localised and patchy erosion. It may be that bed shear stresses are more uniformly distributed in transects across the canyon-channel axis in dense near-bed layers, which more closely resemble hyper-concentrated or debris flows, rather than terrestrial rivers with very low sediment concentrations where outer bend erosion can dominate.

It is clear that knickpoints play a significant role in seabed erosion in the Congo Canyon and indeed elsewhere (Fig. 10A; Heijnen et al., 2020, 2022). Thus, it appears that once topographic irregularities develop on the canyon-channel floor, then they play a key role in focussing subsequent seabed erosion. It is well shown how small-scale topographic 'defects' may focus erosion within much smaller scale scours, at the scale of just a few centimeters to meters (Peakall et al., 2020). But it seems that positive feedbacks leading to focussed erosion can also occur at the scale of hundreds of meters to tens of kilometers.

It may thus be important for models to incorporate the processes that create and maintain knickpoints, especially as submarine knickpoints can migrate at speeds that are up to a million times faster (21 km/yr) than knickpoints in most rivers (0.001 to 1 m/yr; van Heijst and Postma, 2001). Three hypotheses may be put forward for submarine knickpoint formation and maintenance (Heijnen et al., 2022). The first hypothesis is that knickpoints are maintained by instabilities within supercritical flow

('cyclic steps'), but with far longer wavelengths (>1–5 km) than those of the crescent shaped bedforms. The second model is that migrating knickpoints are formed by seabed failures triggered by rapid undrained loading of the substrate, as a turbidity current passes. Rapid rates of sediment accumulation in the depositional areas of the channel floor may favour such failure. Third, once a knickpoint is created, the base of knickpoints may be gradually eroded and undercut by turbidity currents, leading to oversteepening and failure. It is possible that the models are not mutually exclusive. We lack detailed seabed observations of knickpoint generation to test such models, but seabed sediment in parts of the upper Congo Canyon is dominated by cohesive mud (Fig. 11). Thus, knickpoints cannot always be formed by seabed failure via sustained breaching of close-packed and non-cohesive sands, nor liquefaction of loosely-packed sands, although high excess pore pressure and liquefaction might occur in thin and deeply-buried sand layers, or in sand layers deeper than the penetration of available cores.

This work in the Congo Canyon also shows that flank collapses and landslide dams create the largest (up to 150 m high) and longest lasting topographic anomalies and knickpoints (Pope et al., 2022b). In such cases, knickpoint erosion is through remoulded landslide material from the canyon-flank that is dominated by cohesive mud, and may have initially been strongly consolidated before it then failed.

Previous numerical modelling of turbidity currents has often quantified seabed erosion via calculations of excess bed shear stresses, above those needed to initiate erosion (e.g. van Rijn et al., 2019; Halsey, 2018). Such an approach implicitly assumes that sediment is non-cohesive, and that is not the case in the upper Congo Canyon. It is also possible that erosion occurs not via grain-by-grain detachment, but via injection of sediment into the underlying substrate, and delamination of that substrate to form smaller or larger fragments (clasts), as has been inferred from ancient turbidity current outcrops (Eggenhuisen et al., 2011; Fonnesu et al., 2016). In areas with cohesive sediment it is important to constrain changes in sediment shear strength, especially where erosion accesses deeper and more consolidated layers, and account for erosion of blocks of cohesive sediment rather than individual grains or flocs (e.g. Mitchener and Torfs, 1996). Sustained loading and vibration of sediment may also play a role in seabed erosion beneath canyon-flushing turbidity current, which may affect sediment properties and lead to high excess pore pressures, or indeed liquefaction.

These detailed processes are very challenging to monitor in action in the field for turbidity currents, but is clear that turbidity current front speed is not closely linked to depth and volume of erosion (Talling et al., 2022). The fastest flows in the Congo Canyon and Bute Inlet had similar front speeds of 5–8 m/s, yet much more sediment volume was eroded in the Congo Canyon (Talling et al., 2022). Indeed turbidity currents in Monterey Canyon that travelled at up to 7.2 m/s produced subequal amounts of erosion and deposition, typically to depths of <3 m (Paull et al., 2018; Talling et al., 2022). Erosion depths and volumes seem to be more closely related to other flow properties, such as duration of the faster frontal parts of the flows that is highly variable between different field sites (Talling et al., 2023).

Finally, this study of the Congo Canyon may support a hypothesis that submarine canyons locally tend towards a uniform and near-constant gradient (see Section 5.3). Although the underlying reasons why such an equilibrium profile develops are not fully clear, it may also offer opportunities to constrain patterns and depths of local erosion for future turbidity current modelling.

5.4.3. *Interpretation of ancient submarine canyon and channel outcrops*

This study illustrates that thalwegs of active submarine canyons and channel can be extremely dynamic, and undergo large scale changes over very short periods. For example, 82 % of the Congo Canyon and Channel floor underwent changes in elevation of >5 m over just 12 months. Seabed change was dominated by erosion along the floor of the canyon-channel, often to depths of 15–20 m, and with maximum depths of up to 50 m. It is also seen that 20–50 m deep knickpoints can migrate upstream by up to 21 km in just one year during canyon-flushing events, at rates that are around a million times more rapid than typical rates of knickpoint migration in terrestrial rivers (van Heijst and Postma, 2001). These rapid changes are important to consider when looking at the deposits of ancient submarine canyons and channels in outcrop.

The greatest fluctuations in erosion and deposition occur in the vicinity of landslide dams in the upper canyon. Emplacement of the landslide-dam can induce rapid sediment accumulation of up to 150 m in <20 years, with a wedge of sediment extending tens of kilometers upslope from the dam (Pope et al., 2022b). This was followed by knickpoint erosion to depths of up to 50 m within one year. This emphasises the dynamic nature of processes that may built ancient canyon-channel sequences.

Apart from landslide dams, sediment deposition from 2019 to 2020 was typically below the (~5 m) resolution of these ship-mounted bathymetric surveys (5 m in the upper canyon and 15 m in the deep-sea channel). Limited coring of internal terraces and external levees in 2019 (also see Babonneau et al., 2002, 2010) recovered numerous thin-bedded turbidites from such settings, and these areas showed no discernible (<5 m) change from 2019 to 2020. However, a few areas on internal terraces in the upper canyon show >5 m of deposition from 2019 to 2020 (figs. 5 and 8), but these areas are not yet cored, so that the nature of these thicker deposits is uncertain.

This study documents that a very large volume of sediment (equivalent to 19–33 % of the present-day annual sediment flux from rivers to the ocean; Talling et al., 2022) was bypassed down-slope along single or composite erosion surfaces. This emphasises the importance of sediment bypass in submarine canyons and channels (Stevenson et al., 2015). It is consistent with outcrop studies showing that channel-fill deposits can contain numerous erosion and bypass surfaces (Hubbard et al., 2020).

In general, our study suggests that the preservation potential of canyon and channel fill deposits is very low, as previously inferred for smaller scale channels in turbidity current systems (Vendettuoli et al., 2019). However, more bathymetric surveys over a more extended period would be needed to quantify deposited volumes along the canyon-channel axis, as well as eroded volumes, to calculate the exact preservation potential of channel fill deposits. Indeed, quantifying the relative differences in preservation potential across the system requires long-term monitoring due to the relative infrequency of events in the distal channel. Such calculations of deposited sediment volumes are also hampered by the limited resolution of bathymetric surveys in these water depths.

6. Conclusions

This study presents time-lapse bathymetric surveys that show how major submarine canyons and channels in the deep-sea can be carved by powerful 'canyon flushing' turbidity currents. These turbidity currents travelled for 1100 km down the Congo Canyon-Channel in 2020, at speeds of 5–8 m/s (Figs. 1 and 2). The flows eroded a sediment volume of ~2.65 km^3, from a single submarine canyon in one year, which is equivalent to 19–35 % of the global sediment flux from all rivers to the ocean (Talling et al., 2022).

In general, seabed erosion dominated over deposition along the entire canyon-channel, with erosion commonly occurring to depths of 15–20 m over just one year (Figs. 5–7). These surveys also show that seabed erosion is extremely patchy, despite relatively uniform turbidity current flow front speeds of 5–8 m/s (Talling et al., 2021, 2022). This might suggest that local properties of the seafloor may critically impact the depth and rate of erosion, but the small number of sediment cores available from the thalweg of the Congo Canyon-Channel do not support a clear link between dominant facies and depths of erosion, although they do show that erosion in the upper canyon must involve excavation of cohesive sediment (Figs. 11 and 13). Patchy erosion may thus also be largely due to preexisting topographic irregularities, such as steeper knickpoints, which favour deep erosion due to their migration.

Overall, 94 % of the measured seabed erosion occurs on the canyon-channel floor. Of this channel-floor erosion, 22 % is associated with clear knickpoints, and 62 % categorised as general channel floor (thalweg) erosion without such knickpoints, and 10 % is outer bend erosion (Fig. 10; Table 1). The final 6 % of the total volume of erosion is caused by canyon or channel sidewall flank collapses (Table 1), which are most common up-canyon from a major landslide dam that was emplaced before 2019 (Pope et al., 2022b).

The observation that seabed erosion is patchy has important implications for planning submarine cable routes. For example, cable routes should avoid areas close to (or just upstream from) knickpoints, where future seabed erosion may be much deeper. Exchange of sediment with the seabed (i.e. erosion and deposition) will profoundly affect turbidity current behaviour, as it affects the sediment concentration and thus driving force of these flows (Traer et al., 2012; Halsey, 2018). Future modelling of turbidity currents may need to include such localised and patchy seabed erosion, and the underlying processes by which it is generated.

CRediT authorship contribution statement

Sean C. Ruffell: Writing – original draft, Methodology, Investigation, Formal analysis, Conceptualization. **Peter J. Talling:** Writing – review & editing, Writing – original draft, Supervision, Project administration, Methodology, Investigation, Funding acquisition, Formal analysis, Data curation, Conceptualization. **Megan L. Baker:** Writing – review & editing, Supervision, Formal analysis, Conceptualization. **Ed L. Pope:** Writing – review & editing, Formal analysis. **Maarten S. Heijnen:** Writing – review & editing, Formal analysis, Conceptualization. **Ricardo Silva Jacinto:** Writing – review & editing, Supervision. **Matthieu J.B. Cartigny:** Writing – review & editing, Conceptualization. **Stephen M. Simmons:** Formal analysis, Data curation. **Michael A. Clare:** Writing – review & editing, Supervision. **Catharina J. Heerema:** Investigation, Formal analysis. **Claire McGhee:** Investigation. **Sophie Hage:** Writing – review & editing, Investigation. **Martin Hasenhündl:** Investigation, Formal analysis. **Dan R. Parsons:** Investigation, Funding acquisition.

Declaration of competing interest

The authors declare that they have no known competing financial interests or personal relationships that could have appeared to influence the work reported in this paper.

Data availability

2019 and 2020 bathymetric surveys of the Congo Canyon collected on the RRS James Cook and used to inform the erosion calculations are publicly available to download via the British Oceanographic Data Centre (BODC) [https://doi.org/10.5285/dfe7a980-89d8-2830-e053-17d1a68b81ba].

Acknowledgements

The authors acknowledge the efforts of those who helped to collect the bathymetric data that underpins this paper, overcoming a series of major challenges during the covid-19 epidemic. These people include Jez Evans, Natalie Powney, Guy Dale-Smith, Colin Day, Eleanor Darlington, Paul Provost, Mark Maltby of the UK National Marine Facilities, and the officers and crew of the RRS James Cook. Data collection was funded by UK National Environment Research Council (NERC) grants NE/R001952/1 and NE/S010068/1 led by P.J.T., by a Royal Society Dorothy Hodgkin Fellowship (DHF\R1\180166) to M.J.B.C., and Leverhulme Trust Early Career Fellowships to E.L.P and M.L.B (ECF-2018-267 and ECF-2021-566, respectively). Data analysis by S.C.R as part of his doctoral studies was funded via Exxon Mobil. M.C. acknowledges support from NERC COP26 Adaption and Resilience Programme, NERC Climate Linked Atlantic Sector Science (CLASS) National Capability Programme (NE/R015953/1), and the International Cable Protection Committee. The authors confirm that there are no competing interests.

Appendix A. Supplementary data

Supplementary data to this article can be found online at https://doi.org/10.1016/j.geomorph.2024.109350.

References

Allin, J.R., et al., 2016. Different frequencies and triggers of canyon filling and flushing events in Nazaré Canyon, offshore Portugal. Mar. Geol. 371, 89–105. https://doi.org/10.1016/j.margeo.2015.11.005.

Anka, Z., Séranne, M., 2004. Reconnaissance study of the ancient Zaire (Congo) deep-sea fan (ZaiAngo Project). Mar. Geol. 209 (1–4), 223–244. https://doi.org/10.1016/j.margeo.2004.06.007.

Azpiroz-Zabala, M., et al., 2017. Newly recognized turbidity current structure can explain prolonged flushing of submarine canyons. Sci. Adv. 3 (10) https://doi.org/10.1126/sciadv.1700200.

Babonneau, N., et al., 2002. Morphology and architecture of the present canyon and channel system of the Zaire deep-sea fan. Mar. Pet. Geol. 19 (4), 445–467. https://doi.org/10.1016/S0264-8172(02)00009-0.

Babonneau, N., et al., 2010. Sedimentary architecture in meanders of a submarine channel: detailed study of the present Congo Turbidite Channel (Zaiango Project). J. Sediment. Res. 80 (10), 852–866. https://doi.org/10.2110/jsr.2010.078.

Baker, M.L., et al., 2024. Globally significant mass of terrestrial organic carbon efficiently transported by canyon-flushing turbidity currents. Geology. https://doi.org/10.1130/G51976.1.

Baudin, F., et al., 2010. Distribution of the organic matter in the channel-levees systems of the Congo mud-rich deep-sea fan (West Africa). Implication for deep offshore petroleum source rocks and global carbon cycle. Mar. Pet. Geol. 27, 995–1010. https://doi.org/10.1016/j.marpetgeo.2010.02.006.

Bigham, K.T., et al., 2023. Deep-sea benthic megafauna hotspot shows indication of resilience to impact from massive turbidity flow. Front. Mar. Sci. 10, 1180334 https://doi.org/10.3389/fmars.2023.1180334.

Calder, B.R., Mayer, L.A., 2003. Automatic processing of high-rate, high-density multibeam echosounder data. Geochem. Geophys. Geosyst. 4 (6) https://doi.org/10.1029/2002GC000486.

Canals, M., et al., 2006. Flushing submarine canyons. Nature 444 (7117), 354–357. https://doi.org/10.1038/nature05271.

Carter, L., et al., 2009. Submarine Cables and the Oceans: Connecting the World. In: The United Nations Environment Programme World Conservation Monitoring Centre Biodiversity Series. https://doi.org/10.1017/s0002930000266268.

Carter, L., et al., 2014. Insights into submarine geohazards from breaks in subsea telecommunication cables. Oceanography 27 (2), 58–67. https://doi.org/10.5670/oceanog.2014.40.

Clare, M.A., et al., 2016. Preconditioning and triggering of offshore slope failures and turbidity currents revealed by most detailed monitoring yet at a fjord-head delta. Earth Planet. Sci. Lett. 450, 208–220. https://doi.org/10.1016/j.epsl.2016.06.021.

Covault, J.A., Graham, S.A., 2010. Submarine fans at all sea-level stands: tectono-morphologic and climatic controls on terrigenous sediment delivery to the deep sea. Geology 38 (10), 939–942. https://doi.org/10.1130/G31081.1.

Coynel, A., et al., 2005. Spatial and seasonal dynamics of total suspended sediment and organic carbon species in the Congo River. Global Biogeochem. Cycles 19 (4), 1–17. https://doi.org/10.1029/2004GB002335.

Dennielou, B., et al., 2017. Morphology, structure, composition and build-up processes of the active channel-mouth lobe complex of the Congo deep-sea fan with inputs from remotely operated underwater vehicle (ROV) multibeam and video surveys. Deep-Sea Res. II Top. Stud. Oceanogr. 142, 25–49. https://doi.org/10.1016/j.dsr2.2017.03.010.

Eggenhuisen, J.T., et al., 2011. Shallow erosion beneath turbidity currents and its impact on the architectural development of turbidite sheet systems. Sedimentology 58, 936–959. https://doi.org/10.1111/j.1365-3091.2010.01190.x.

Ferry, J.N., et al., 2004. Morphogenesis of Congo submarine canyon and valley: Implications about the theories of the canyons formation. Geodin. Acta 17 (4), 241–251. https://doi.org/10.3166/ga.17.241-251.

Fonnesu, M., et al., 2016. Hybrid event beds generated by local substrate delamination on a confined-basin floor. J. Sediment. Res. 86, 929–943. https://doi.org/10.2110/jsr.2016.58.

Gardner, T.W., 1984. Experimental study of knickpoint and longitudinal profile evolution in cohesive, homogeneous material: reply. Bull. Geol. Soc. Am. 95 (1), 123. https://doi.org/10.1130/0016-7606(1984)95<123:ESOKAL>2.0.CO;2.

Guiastrennec-Faugas, L., et al., 2020. Upstream migrating knickpoints and related sedimentary processes in a submarine canyon from a rare 20-year morphobathymetric time-lapse (Capbreton submarine canyon, Bay of Biscay, France). Mar. Geol. 423 https://doi.org/10.1016/j.margeo.2020.106143.

Hage, S., et al., 2018. How to recognize crescentic bedforms formed by supercritical turbidity currents in the geologic record: insights from active submarine channels. Geology 46 (6), 563–566. https://doi.org/10.1130/G40095.1.

Hage, S., et al., 2020. Efficient preservation of young terrestrial organic carbon in sandy turbidity current deposits. Geology 48, 882–887. https://doi.org/10.1130/G47320.1.
Hage, S., et al., 2022. Turbidity currents can dictate organic carbon fluxes across river-fed fjords: an example from Bute Inlet (BC, Canada). J. Geophys. Res. Biogeosci. e2022JG006824 https://doi.org/10.1029/2022JG006824.
Hage, S., et al., 2024. How is particulate organic carbon transported through the river-fed Congo Submarine Canyon to the deep-sea? Biogeosciences. https://doi.org/10.5194/egusphere-2024-900 (MS - egusphere-2024-900).
Halsey, T.C., 2018. Erosion of unconsolidated beds by turbidity currents. In: Physical Review Fluids. American Physical Society. https://doi.org/10.1103/PhysRevFluids.3.104303.
Hay, W.W., 1998. Detrital sediment fluxes from continents to oceans. Chem. Geol. 145 (3–4), 287–323. https://doi.org/10.1016/S0009-2541(97)00149-6.
Heerema, C.J., et al., 2020. What determines the downstream evolution of turbidity currents? Earth Planet. Sci. Lett. 532, 116023 https://doi.org/10.1016/j.epsl.2019.116023.
Heezen, B.C., Ewing, W.M., 1952. Turbidity currents and submarine slumps, and the 1929 Grand Banks [Newfoundland] earthquake. Am. J. Sci. 250 (12), 849–873. https://doi.org/10.2475/ajs.250.12.849.
Heijnen, M.S., et al., 2020. Rapidly-migrating and internally-generated knickpoints can control submarine channel evolution. Nat. Commun. 11 (1) https://doi.org/10.1038/s41467-020-16861-x.
Heijnen, M.S., et al., 2022. Fill, flush or shuffle: how is sediment carried through submarine channels to build lobes? Earth Planet. Sci. Lett. 584, 117481 https://doi.org/10.1016/j.epsl.2022.117481.
Heiniö, P., Davies, R.J., 2007. Knickpoint migration in submarine channels in response to fold growth, western Niger Delta. Mar. Pet. Geol. 24, 434–449. https://doi.org/10.1016/j.marpetgeo.2006.09.002.
Hodgson, D.L., et al., 2011. Submarine slope degradation and aggradation and the stratigraphic evolution of channel–levee systems. J. Geol. Soc. London 168, 625–628. https://doi.org/10.1144/0016-76492010-177.
Howard, A.D., et al., 1994. Modeling fluvial erosion on regional to continental scales. J. Geophys. Res. 99 (B7) https://doi.org/10.1029/94jb00744.
Hubbard, S.M., et al., 2020. The stratigraphic evolution of a submarine channel: linking seafloor dynamics to depositional products. J. Sediment. Res. 90 (7), 673–686. https://doi.org/10.2110/jsr.2020.36.
Hughes Clarke, J.E., 2016. First wide-angle view of channelized turbidity currents links migrating cyclic steps to flow characteristics. Nat. Commun. 7 (May) https://doi.org/10.1038/ncomms11896.
Migeon, S., et al., 2004. Processes of sediment-wave construction along the present Zaire deep-sea meandering channel: Role of meanders and flow stripping. J. Sediment. Res. 74, 580–598. https://doi.org/10.1306/091603740580.
Mitchener, H., Torfs, H., 1996. Erosion of mud/sand mixtures. Coast. Eng. 29, 1–25. https://doi.org/10.1016/S0378-3839(96)00002-6.
Mountjoy, J.J., et al., 2018. Earthquakes drive large-scale submarine canyon development and sediment supply to deep-ocean basins. Sci. Adv. 4 (3), 1–9. https://doi.org/10.1126/sciadv.aar3748.
Normark, W.R., Carlson, P.R., 2003. Giant submarine canyons: is size any clue to their importance in the rock record? Geol. Soc. Am. Spec. Pap. 370, 175–190. https://doi.org/10.1130/0-8137-2370-1.175.
Normark, W.R., Piper, D.J.W., 1991. Initiation processes and flow evolution of turbidity currents: implications for the depositional record. In: Osborne, R.H. (Ed.), From Shoreline to Abyss: Contributions in Marine Geology in Honor of Francis Parker Shepard. SEPM Society for Sedimentary Geology, p. 0. https://doi.org/10.2110/pec.91.09.0207.
Normandeau, A., et al., 2020. Storm-induced turbidity currents on a sediment-starved shelf: Insight from direct monitoring and repeat seabed mapping of upslope migrating bedforms. Sedimentology 67, 1045–1068. https://doi.org/10.1111/sed.12673.
Normark, W.R., et al., 1993. Turbidite systems: state of the art and future directions. Rev. Geophys. 31, 91–116. https://doi.org/10.1029/93RG02832.
Palm, F.A., et al., 2021. Width variation around submarine channel bends: implications for sedimentation and channel evolution. Mar. Geol. 437, 106504 https://doi.org/10.1016/j.margeo.2021.106504.
Parker, G., 1982. Conditions for the ignition of catastrophically erosive turbidity currents. Mar. Geol. 46 (3–4), 307–327. https://doi.org/10.1016/0025-3227(82)90086-X.
Parker, G., et al., 1986. Self-accelerating turbidity currents. J. Fluid Mech. 171, 145–181. https://doi.org/10.1017/S0022112086001404.
Paull, C.K., et al., 2011. High-resolution bathymetry of the axial channels within Monterey and Soquel submarine canyons, offshore central California. Geosphere 7 (5), 1077–1101. https://doi.org/10.1130/GES00636.1.
Paull, C.K., et al., 2013. Anatomy of the La Jolla Submarine Canyon system; offshore southern California. Mar. Geol. 335, 16–34. https://doi.org/10.1016/j.margeo.2012.10.003.
Paull, C.K., et al., 2018. Powerful turbidity currents driven by dense basal layers. Nat. Commun. 9 (1) https://doi.org/10.1038/s41467-018-06254-6.
Peakall, J., Sumner, E.J., 2015. Submarine channel flow processes and deposits: a process-product perspective. Geomorphology 244, 95–120. https://doi.org/10.1016/j.geomorph.2015.03.005.
Peakall, J., et al., 2020. An integrated process-based model of flutes and tool marks in deep-water environments: implications for palaeohydraulics, the Bouma sequence, and hybrid event beds. Sedimentology 67, 1601–1666. https://doi.org/10.1111/sed.12727.
Peters, J., 1978. Discharge and sand transport in the braided zone of the Zaire Estuary. Neth. J. Sea Res. 183 (3), 341–358. https://doi.org/10.1016/0077-7579(78)90031-5.
Picot, M., et al., 2016. Controls on turbidite sedimentation: insights from a quantitative approach of submarine channel and lobe architecture (Late Quaternary Congo Fan). Mar. Pet. Geol. 72, 423–446. https://doi.org/10.1016/j.marpetgeo.2016.02.004.
Picot, M., et al., 2019. Monsoon control on channel avulsions in the Late Quaternary Congo Fan. Quat. Sci. Rev. 204, 149–171. https://doi.org/10.1016/j.quascirev.2018.11.033.
Piper, D.J.W., Savoye, B., 1993. Processes of late Quaternary turbidity current flow and deposition on the Var deep-sea fan, north-west Mediterranean Sea. Sedimentology 40 (3), 557–582. https://doi.org/10.1111/j.1365-3091.1993.tb01350.x.
Piper, D.J.W., Cochonat, P., Morrison, 1999. The sequence of events around the epicentre of the 1929 Grand Banks earthquake: initiation of debris flows and turbidity current inferred from sidescan sonar. Sedimentology 46, 79–97. https://doi.org/10.1046/j.1365-3091.1999.00204.x.
Pope, E.L., et al., 2022a. First source-to-sink monitoring shows dense head determines sediment gravity flow runout. Sci. Adv. 8, eabj3220 https://doi.org/10.1126/sciadv.abj3220.
Pope, E.L., et al., 2022b. Carbon and sediment fluxes inhibited in the submarine Congo Canyon by landslide-damming. Nat. Geosci. 15, 845–853. https://doi.org/10.1038/s41561-022-01017-x.
Rabouille, C., et al., 2017. The Congolobe project, a multidisciplinary study of Congo deep-sea fan lobe complex: overview of methods, strategies, observations and sampling. Deep-Sea Res. II Top. Stud. Oceanogr. 142 (May), 7–24. https://doi.org/10.1016/j.dsr2.2016.05.006.
Savoye, B., et al., 2000. Structure et évolution récente de l'éventail turbiditique du Zaïre: premiers résultats scientifiques des missions d'exploration Zaïango 1 & 2 (marge Congo-Angola) Abridged version.
Savoye, B., et al., 2009. Geological overview of the Angola-Congo margin, the Congo deep-sea fan and its submarine valleys. Top. Stud. Oceanogr. 56 (23) https://doi.org/10.1016/j.dsr2.2009.04.001ï.
Sawyer, D.E., DeVore, J.R., 2015. Elevated shear strength of sediments onactive margins: evidence for seismic strengthening. Geophys. Res. Lett. 42, 10216–10221. https://doi.org/10.1002/2015GL066603.
Schimel, A.C.G., et al., 2015. Accounting for uncertainty in volumes of seabed change measured with repeat multibeam sonar surveys. Cont. Shelf Res. 111, 52–68. https://doi.org/10.1016/j.csr.2015.10.019.
Sequeiros, O.E., et al., 2019. How typhoons trigger turbidity currents in submarine canyons. Sci. Rep. 9, 9220. https://doi.org/10.1038/s41598-019-45615-z.
Simmons, S.M., et al., 2020. Novel acoustic method provides first detailed measurements of sediment concentration structure within submarine turbidity currents. J. Geophys. Res. 125, e2019JC015904 https://doi.org/10.1029/2019JC015904.
Stevenson, C.J., et al., 2015. Deep-water sediment bypass. J. Sediment. Res. 85, 1058–1081. https://doi.org/10.2110/jsr.2015.63.
Syvitski, J., et al., 2022. Earth's sediment cycle during the Anthropocene. Nat. Rev. Earth Environ. 3 (3), 179–196. https://doi.org/10.1038/s43017-021-00253-w.
Talling, P.J., et al., 2012. Subaqueous sediment density flows: Depositional processes and deposit types. Sedimentology 59 (7), 1937–2003. https://doi.org/10.1111/j.1365-3091.2012.01353.x.
Talling, P.J., et al., 2021. Novel sensor array helps to understand submarine cable faults off West Africa Novel sensor array helps to understand submarine cable faults off West Africa. In: White Paper on Submarine Cable Geohazards archived on Earthxiv, pp. 1–26. https://doi.org/10.31223/X5W328.
Talling, P.J., et al., 2022. Longest sediment flows yet measured show how major rivers connect effi ciently to deep sea. Nat. Commun. 13 (4193), 1–15. https://doi.org/10.1038/s41467-022-31689-3.
Talling, P.J., et al., 2023. Detailed monitoring reveals the nature of submarine turbidity currents. Nat. Rev. Earth Environ. https://doi.org/10.1038/s43017-023-00458-1.
Talling, P.J., et al., 2024. The global turbidity current pump and its implications for organic carbon cycling. Annu. Rev. Mar. Sci. 16 https://doi.org/10.1146/annurev-marine-032223-103626 (8.1–8.29).
Traer, M.M., et al., 2012. The sensitivity of turbidity currents to mass and momentum exchanges between these underflows and their surroundings. J. Geophys. Res. Earth 117 (1). https://doi.org/10.1029/2011JF001990.
van Heijst, M.W.I.M., Postma, G., 2001. Fluvial response to sea-level changes: a quantitative analogue, experimental approach. Basin Res. 13, 269–292. https://doi.org/10.1046/j.1365-2117.2001.00149.x.
Van Rijn, L.C., et al., 2019. Modified sediment pick-up function. J. Hydraul. Eng. 145 (1), 06018017 https://doi.org/10.1061/(ASCE)HY.1943-7900.0001549.
Vangriesheim, A., Khripounoff, A., Crassous, P., 2009. Turbidity events observed in situ along the Congo submarine channel. Deep-Sea Res. II Top. Stud. Oceanogr. 56 (23), 2208–2222. https://doi.org/10.1016/j.dsr2.2009.04.004.
Vendettuoli, D., et al., 2019. Daily bathymetric surveys document how stratigraphy is built and its extreme incompleteness in submarine channels. Earth Planet. Sci. Lett. 515, 231–247. https://doi.org/10.1016/j.epsl.2019.03.033.
Wang, Z., et al., 2020. Direct evidence of a high-concentration basal layer in a submarine turbidity current. Deep-Sea Res. I (April), 103300. https://doi.org/10.1016/j.dsr.2020.103300.
Wolfson-Schwehr, M., et al., 2023. Time-lapse Seafloor surveys reveal how turbidity currents and internal tides in Monterey Canyon interact with the seabed at centimeter-scale. J. Geophys. Res. Earth 128, e2022JF006705. https://doi.org/10.1029/2022JF006705.